THE GEOLOGICAL SOCIETY OF AMERICA®

Response of larger benthic foraminifera to the Paleocene-Eocene thermal maximum and the position of the Paleocene/Eocene boundary in the Tethyan shallow benthic zones: Evidence from south Tibet

Qinghai Zhang[1,2,†], Helmut Willems[2,3], Lin Ding[1], and Xiaoxia Xu[2]

[1]*Key Laboratory of Continental Collision and Plateau Uplift, Institute of Tibetan Plateau Research, and CAS Centre for Excellence in Tibetan Plateau Earth Sciences, Lincui Road 16-3, 100101 Beijing, China*

[2]*Department of Geosciences, University of Bremen, Klagenfurter Straße 4, 28359 Bremen, Germany*

[3]*Nanjing Institute of Geology and Palaeontology, Chinese Academy of Sciences, East Beijing Road 39, 210008 Nanjing, China*

ABSTRACT

The Paleocene-Eocene thermal maximum (PETM) is one of the most pronounced global warming events in the Cenozoic. This event was associated with a large negative carbon isotope excursion (CIE) and with major changes in the atmosphere, hydrosphere, and biosphere. However, how the larger benthic foraminifera (LBFs) in the shallow Tethyan Ocean responded to the PETM remains controversial. In this study, we investigate two shallow-marine, LBF-rich carbonate sections from south Tibet, aiming to locate the position of the Paleocene/Eocene (P/E) boundary in the Tethyan shallow benthic zones (SBZs) and to examine the response of the LBFs to the PETM. Carbon isotope compositions of bulk carbonate were measured to constrain the stratigraphic position of the CIE onset marking the P/E boundary in the sections, and the LBFs were studied in rock thin sections in order to assess their biostratigraphy and to construct the SBZs. The combination of the carbon isotope data and constructed SBZs shows that the P/E boundary is located within SBZ5, not at the SBZ4/SBZ5 transition as proposed in the Western Tethyan domain. At the P/E boundary, no evident compositional change in LBF assemblages can be observed. However, a major compositional change in LBF assemblages occurs in the CIE recovery, characterized by the sudden disappearance of *Miscellanea*, *Ranikothalia*, *Setia*, *Orbitosiphon*, and the initial dominance of porcellaneous-walled *Alveolina* and *Orbitolites* together with small miliolids and rotaliids. We tentatively speculate that this compositional change in LBF assemblages may be related to a eutrophication event, likely resulting from intensified continental weathering during the CIE recovery of the PETM.

INTRODUCTION

About 56 m.y. ago, global temperature rose rapidly by at least 4–5 °C (Zachos et al., 2003; Dunkley Jones et al., 2013), and this temperature anomaly persisted for ~170 k.y. (Röhl et al., 2007). This event, now called the Paleocene-Eocene thermal maximum (PETM), was associated with severe carbonate dissolution on the deep-sea floor (Zachos et al., 2005) and with a ~2–7‰ negative carbon isotope excursion (CIE) (McInerney and Wing, 2011), indicating a massive addition of ^{13}C-depleted carbon into the atmosphere-ocean system (Dickens et al., 1995). The CIE was documented by diverse substrates from different depositional environments, ranging from paleosol carbonate, tooth enamel, plant lipids, soil organic matter on land to foraminifera, bulk carbonate, and marine organic matter in the ocean (McInerney and Wing, 2011). Therefore, the CIE reflects a global geochemical event, and not a regional carbon perturbation. In addition, the CIE onset was thought to have happened within ≤5 k.y. (Farley and Eltgroth, 2003; Röhl et al., 2007; Zeebe et al., 2009). Its omnipresence and geological instantaneity make the CIE onset a very accurate time marker for inter-regional stratigraphic correlation. Consequently, the CIE onset was officially selected as the criterion for defining the Paleocene/Eocene (P/E) boundary (Aubry and Ouda, 2003).

Along with the PETM-CIE, dramatic changes took place in the ocean-atmosphere system, such as a marked increase in atmospheric CO_2 concentration (Archer, 2010), intensified seasonal precipitation and weathering (Schmitz and Pujalte, 2007; Chen et al., 2016; Penman, 2016), abrupt reversal of deep-ocean circulation (Tripati and Elderfield, 2005), rapid ocean acidification (Zachos et al., 2005; Zeebe et al., 2009), and increased ocean stratification (Winguth et al., 2012). In different ecosystems, fauna and flora showed variable responses to this warming event. On land, insect herbivory increased sharply (Currano et al., 2008) as floral composition changed from mixed gymnosperms and angiosperms prior to the PETM to almost exclusively angiosperms during the PETM (Wing et al., 2005). Many mammals became smaller (Secord et al., 2012), and migrated from Asia to North America (Bowen et al., 2002). In the tropical surface ocean, reef-building corals retreated to middle latitudes (Scheibner and Speijer, 2008), planktonic foraminifera diversified rapidly (Kelly et al., 1996), and calcareous nannoplankton experienced increased rates of origination and extinction (Gibbs et al., 2006). In the deep ocean, smaller benthic foraminifera suffered one of the largest extinctions in the Cenozoic with the loss of ~30%–50% species (Thomas and Shackleton, 1996; Speijer et al., 1997).

Despite substantial progress in the PETM studies, how larger benthic foraminifera (LBFs) in the shallow Tethyan Ocean responded to the PETM is still debated. In 1998, Hottinger (1998) coined the term "larger foraminiferal turnover" (LFT), defined as the start of adult dimorphism and large shell size. Afterward, some authors suggested that this LFT event coincided with the PETM and further postulated a causal relationship between the PETM and the LFT (Orue-Etxebarria et al., 2001; Pujalte et al., 2009; Scheibner and Speijer, 2009). This view, however, is controversial as other authors have argued that the LFT predates the PETM (Hottinger, 1998; Zhang et al., 2013) and is not directly related to the PETM (Hottinger, 1998;

†zhang@itpcas.ac.cn

GSA Bulletin; January/February 2019; v. 131; no. 1/2; p. 84–98; https://doi.org/10.1130/B31813.1; 9 figures; Data Repository item 2018215; published online 1 August 2018.

Zamagni, 2009; Zhang et al., 2013). According to the definition given by Hottinger (1998), the LFT does not represent a catastrophic event. Instead, it refers to an evolutionary success of some extreme K-strategist LBFs that were exploiting seasonal changes in nutrient input after their adaptation to seasonality in warm, oligotrophic environments (Hottinger, 1998). During the PETM, a short-term eutrophication, resulting from increased seasonal precipitation and continental weathering (Schmitz and Pujalte, 2007; Chen et al., 2016), occurred in the coastal environments (Scheibner et al., 2005; Stassen, et al., 2009, 2012), and the occurrence of eutrophication is immediately fatal for the development of symbiont-bearing LBFs (Hottinger, 1998). Although the eutrophication might not be omnipresent in the Tethyan Ocean, it is still puzzling why the evolutionary success of the LBFs seems to have coincided with this environmentally unstable period of the PETM.

Aside from the relationship between the PETM and the LFT, the exact position of the P/E boundary in the Tethyan shallow benthic zones (SBZs) is also debated. Some authors proposed that the P/E boundary should be placed at the SBZ4/SBZ5 transition (Pujalte et al., 2009; Scheibner and Speijer, 2009; Zamagni et al., 2012), whereas others suggested that it was stratigraphically higher than the SBZ4/SBZ5 transition, either within SBZ5 (Zhang et al., 2013) or within a long stratigraphic range between the upper SBZ5 and the lower SBZ7 (Serra-Kiel et al., 1998; Hottinger, 2001). The allocation of this long range (SBZ5-SBZ7) for the P/E boundary was partly because an agreement on the definition of the P/E boundary was not reached at that time.

A prerequisite to solving the aforementioned problems is to study complete shallow-marine sections that preserve high-resolution CIE records and contain plenty of in situ diagnostic LBFs. Unfortunately, it appears that some studied sections from Spain and Egypt do not meet these requirements, because they either comprise non-marine sediments or contain reworked LBFs in the stratigraphic interval close to the P/E boundary (Pujalte et al., 2009; Scheibner and Speijer, 2009). In addition, the designation of the P/E boundary in sections depends on the recognition of the CIE onset, and it has been suggested that the CIE onset took place within ≤5 k.y. (Farley and Eltgroth, 2003; Röhl et al., 2007; Zeebe et al., 2009). Thus, even for some fully marine carbonate sections with in situ LBFs, whether these sections are "complete" on millennial time scales and have preserved carbonate sediments produced in this geologically brief time interval is also vital to the precise designation of the P/E boundary and to understanding of the LBF response to the PETM.

In this work, we present carbon isotope data measured from bulk carbonate ($\delta^{13}C_{carb}$) samples that were collected from two shallow-marine carbonate sections (sections 13ZS at Tingri and 11TMG at Gamba) in south Tibet, and the $\delta^{13}C_{carb}$ data from section 13ZS were recently published to discuss the nature of the CIE (Zhang et al., 2017). Then, we consider possible effects of diagenesis and local processes on the $\delta^{13}C_{carb}$ records and discuss the stratigraphic completeness of the PETM-CIE interval in the sections. In summary, we construct a LBF biostratigraphy, pinpoint the P/E boundary in the SBZs, and discuss the LBF response to the PETM.

GEOLOGICAL SETTING AND STRATIGRAPHY

Sections 13ZS and 11TMG are located in the Tingri and Gamba areas, respectively, tectonostratigraphically within the southern Tethyan Himalaya. The Tethyan Himalaya represents the northernmost Greater Indian continental margin and separates from High Himalaya to the south by South Tibet Detachment System and from Lhasa Terrane to the north by the Indus-Yarlung Zangbo Suture (Fig. 1). During the Paleocene and early Eocene, the Tethyan Himalaya was situated in the tropical Tethyan Ocean with a latitude of ~10 °N (van Hinsbergen et al., 2012). At that time, carbonate sediments rich in LBFs were deposited in the shallow-marine environment of the southern Tethyan Himalaya (Willems et al., 1996; Zhang et al., 2013), while quartz-rich siliciclastic sedi-

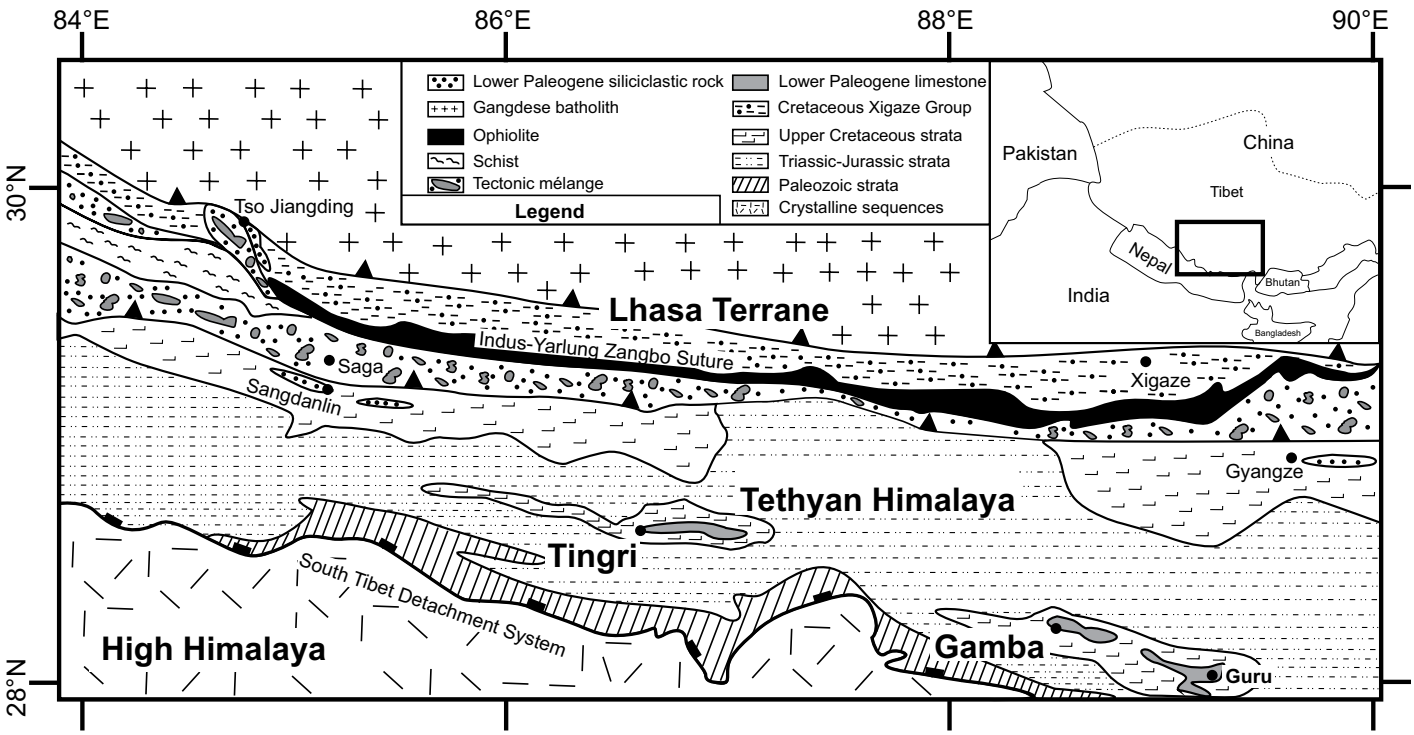

Figure 1. Schematic geological map of south Tibet showing the studied areas of Tingri and Gamba (modified after Zhang et al. 2013).

ments and radiolarian-bearing cherts were deposited in the deep-water environments of the northern Tethyan Himalaya (Ding et al., 2005). Subsequently, post–50 Ma India-Asia convergence caused a great amount of upper crustal shortening (van Hinsbergen et al., 2012), leading to significant uplift and severe erosion of sedimentary records in the Tethyan Himalaya. As a consequence, the lower Paleogene carbonate rocks were removed from most parts of the southern Tethyan Himalaya so that they crop out now only in a few areas, such as Tingri, Gamba, and Guru (Fig. 1).

In the Tingri area, an ~400-m-thick carbonate sequence of the Zhepure Shan Formation is exposed in the Shenkeza valley that lies ~4 km NE of the Youxia village and ~15 km NE of the Tingri county (Fig. 2). The Zhepure Shan Formation overlies the quartz sandstone of the Jidula Formation and underlies the green shales/marls of the Youxia Formation. The Zhepure Shan Formation can be divided into four informal lithological members: cyclic limestone of the Member A, massive limestone of the Member B, nodular limestone of the Member C, and massive limestone of the Member D. Carbonate sequences from the upper Member A to the Member D are rich in LBFs, and previous study of these LBF assemblages indicates that the Zhepure Shan Formation roughly covers a stratigraphic interval of SBZ1-SBZ10 (~62–52 m.y.), with the P/E boundary in the upper Member C (Zhang et al., 2013).

In the Gamba area, the Zongpu Formation is ~200 m thick and exposed in the Zongpu valley, ~1.5 km NE of the Gamba county (Fig. 2). Similar to Tingri, the Zongpu Formation is intercalated between the underlying quartz sandstone of the Jidula Formation and the overlying green marls of the Zongpubei Formation. Carbonate sequences of the Zongpu Formation were strongly folded by tectonic forces so that the expression of four lithological members can only be recognized by integration of several discrete sections. Compared with the Zhepure Shan Formation, the Zongpu Formation represents a shorter time interval, from SBZ2 to SBZ7 (~60–54 m.y.), and the P/E boundary is located within the lower Member D (Zhang et al., 2013).

SECTIONS AND METHODS

In this study, we logged section 13ZS at Tingri (N28°41′35″, E86°42′32″) and section 11TMG at Gamba (N28°17′01″, E88°31′47″) (Figs. 3 and 4). Both sections are ~20 m thick, covering the key stratigraphic interval of the uppermost Paleocene and the lowermost Eocene. At Tingri, carbonate rock in section 13ZS consists of calcareous marl, nodular marl, nodular limestone, and limestone (Fig. 3). Below ~7 m in the section, the lithology varies repeatedly from nodular marl to nodular limestone/limestone. Between ~7 m and 18.4 m in the section, carbonate rock is composed of purely nodular limestone, and the nodular limestone consists of sub-rounded, decimeter-sized nodules that are densely packed and show a fitted-fabric texture (Fig. 5A). Above 18.4 m in the section, intercalations of thick-bedded nodular limestone and thin-layered marl appear repeatedly.

At Gamba, carbonate rock in section 11TMG consists of nodular marl, nodular limestone, limestone, and conglomerate (Fig. 4). Below ~6 m in the section, it consists of unevenly bedded nodular limestone (Fig. 5B). Between ~6 m and 19 m in the section, there are three lithological units, each composed of nodular marl at the bottom, nodular limestone in the middle and thin-bedded limestone at the top (Figs. 5C and 5D). Immediately overlying these units is a thin conglomerate layer, where brownish limestone pebbles rich in SBZ5 LBFs (*Miscellanea*, *Ranikothalia*, *Operculina*) float in the yellowish carbonate matrix with SBZ6 LBFs (*Alveolina*, *Orbitolites*) (Fig. 5F). No siliciclastic sediments derived from beyond the carbonate ramp can be observed in this conglomerate layer. This implies that the conglomerate was likely formed by erosion of locally uplifted or exposed SBZ5 limestone and transport of SBZ5 limestone pebbles into the neighboring carbonate ramp. Upward, the conglomerate layer is capped with thick-bedded, massive *Alveolina* limestone at the top (Fig. 5E).

In the field, we sampled every ~20 cm in the sections and >200 samples were collected. For each sample, at least one thin section, measuring 8 × 10 cm or even larger, was polished to study the LBFs (Figs. 6 and 7). For $\delta^{13}C$ and $\delta^{18}O$

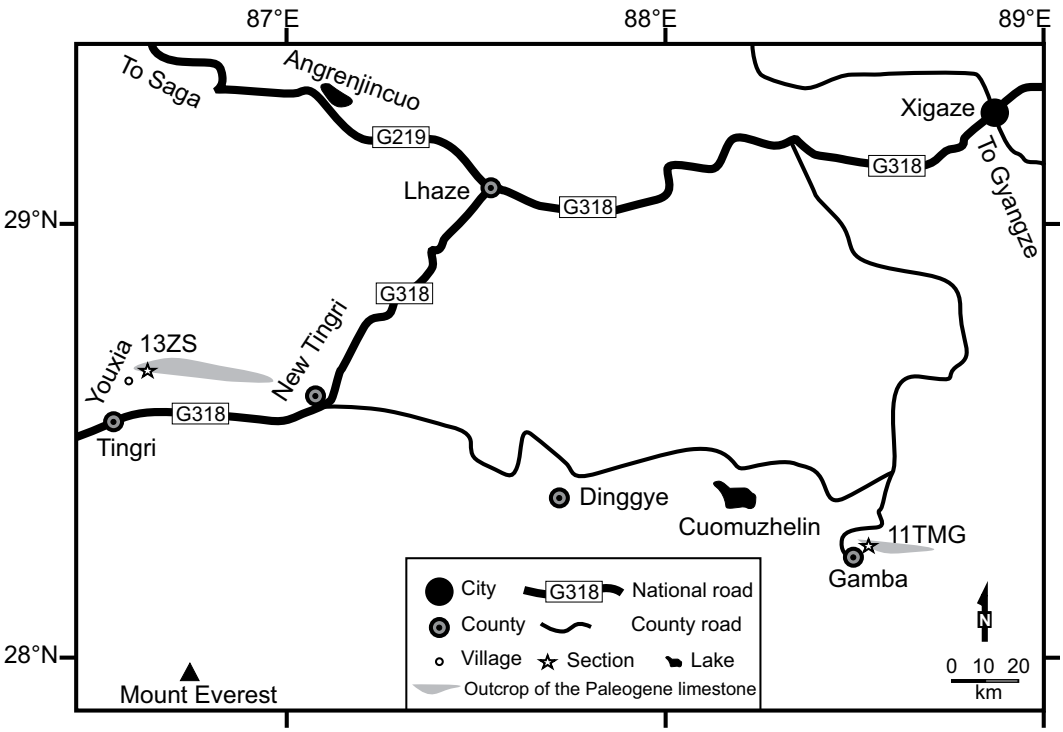

Figure 2. Simplified geographical map showing locations of two studied sections.

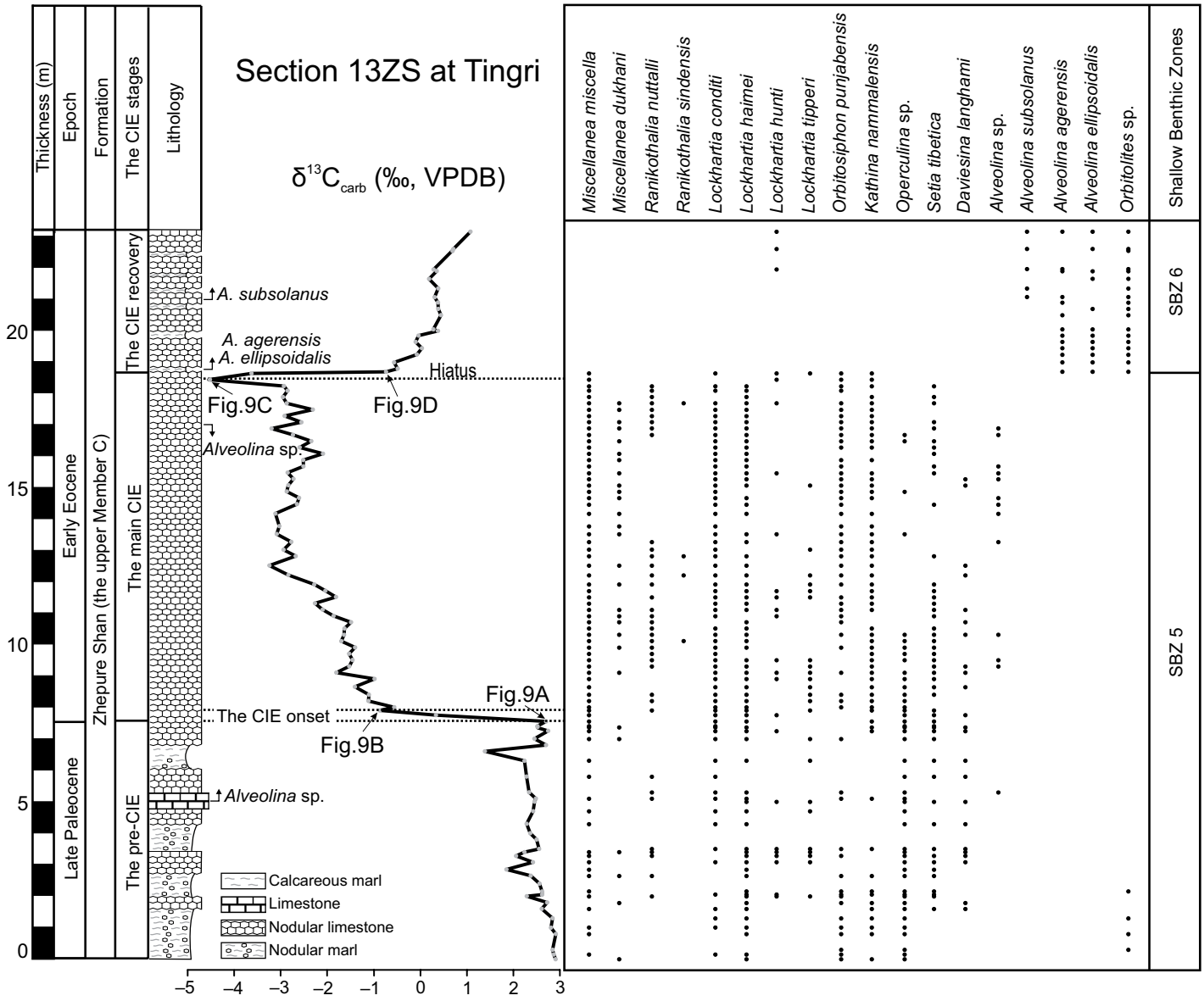

Figure 3. Lithology, bulk $\delta^{13}C_{carb}$ record and stratigraphic distribution of larger benthic foraminifer taxa in section 13ZS. Dashed lines delimit intervals of the carbon isotope excursion (CIE) onset and the main CIE. Arrows by the CIE profile indicate stratigraphic positions of four photomicrographs shown in Figure 9.

analyses, samples were cut to expose their fresh surfaces. On their fresh surfaces, diagenetically less-altered micrites and LBF fragments were carefully micro-drilled under a light microscope. Veins, vugs, and petrographically visible diagenetic parts were strictly avoided. About 20 g of material was obtained from each sample and then ground to powder in an agate mortar. For $\delta^{13}C$ and $\delta^{18}O$ measurements, ~100 µg of rock powder were reacted with phosphoric acid at 75 °C in an automated carbonate unit. The isotopic composition ($\delta^{13}C$, $\delta^{18}O$) of the resulting CO_2 was measured with a Finnigan MAT 251 gas isotope ratio mass spectrometer at the MARUM, University of Bremen. An analytical precision of ± 0.05‰ (±1 standard deviation) for $\delta^{13}C$ and ± 0.07‰ (±1 standard deviation) for $\delta^{18}O$ measurements was determined for this instrument based on replicate analyses of an in-house standard (Solnhofen limestone). This in-house standard was calibrated to the international standard NBS 19. All isotope-ratio data are reported by using the per mil (‰) versus VPDB (Vienna Peedee Belemnite) notation (Table DR1).[1]

DISCUSSIONS

Data Evaluation

Previous studies suggested that $\delta^{13}C_{carb}$ variations in limestone may not reflect the $\delta^{13}C$ changes of local seawater in which biogenic calcium carbonates were originally precipitated, because of the effects of diagenesis and mixed different components (Banner and Hanson,

[1]GSA Data Repository item 2018215, carbon and oxygen isotope data of bulk carbonate from section 11TMG (Table DR1), is available at http://www.geosociety.org/datarepository/2018 or by request to editing@geosociety.org.

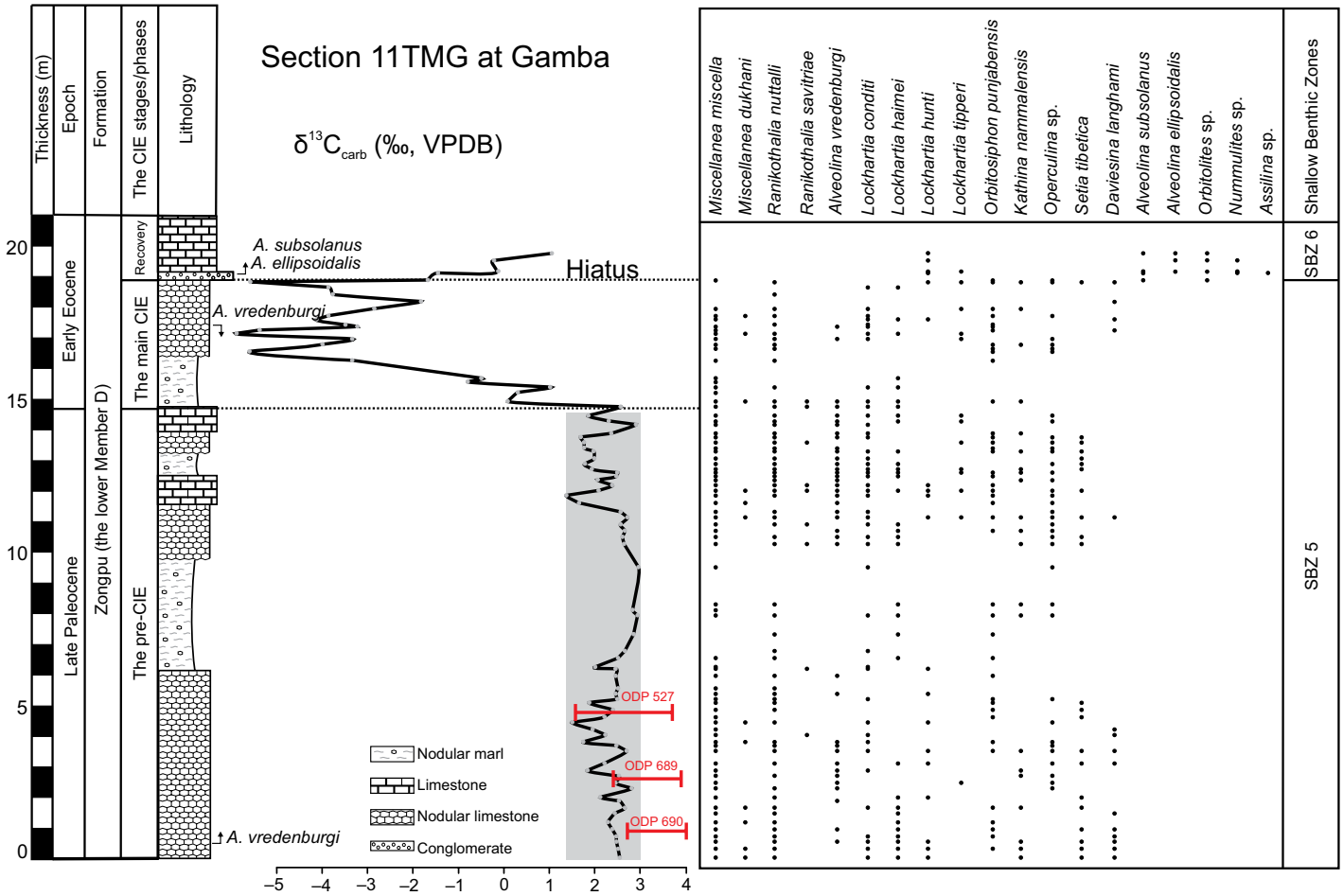

Figure 4. Lithology, bulk $\delta^{13}C_{carb}$ record and stratigraphic distribution of larger benthic foraminifer taxa in section 11TMG. Two dashed lines delimit the stratigraphic interval of the main carbon isotope excursion (CIE). Grey shading shows the range of the pre-CIE $\delta^{13}C_{carb}$ variations in section 13ZS. Red horizontal lines represent ranges of the pre-CIE $\delta^{13}C$ variations from surface-dwelling planktonic foraminifer *Acarinina* at Ocean Drilling Program sites. The $\delta^{13}C$ data of *Acarinina* are sourced from Thomas et al. (1999), Thomas et al. (2002), and Zachos et al. (2007).

1990; Sluijs and Dickens, 2012). Diagenetic overprinting resulting from chemical exchange with meteoric water, water-rock interaction in an open system, or the transformation of unstable aragonite into low-Mg calcite typically lowers $\delta^{13}C$ values (Banner and Hanson, 1990; Swart and Eberli, 2005). As a consequence, the $\delta^{13}C_{carb}$ of the diagenetically altered limestone is usually more ^{13}C-depleted than the $\delta^{13}C$ of original carbonate sediments (Banner and Hanson, 1990). Besides, marine bulk carbonate consists of different components (e.g., micrites, algae, foraminifera, coccoliths). If $\delta^{13}C$ values of these components vary largely, the measured $\delta^{13}C_{carb}$ values would be affected by relative abundance of the mixed components. This being the case, then, variations of the measured $\delta^{13}C_{carb}$ may not reflect changes in the seawater $\delta^{13}C$ (Swart and Eberli, 2005). In addition, seawater $\delta^{13}C$ in some shallow epeiric seas might also be complicated by local processes, such as freshwater discharge, evaporation, and oxidation of organic matter (Patterson and Walter, 1994; Panchuk et al., 2006; Immenhauser et al., 2008). Thus, the $\delta^{13}C$ ratios measured from shallow-water bulk carbonate samples should be carefully examined before they are used to reconstruct secular variations in the $\delta^{13}C$ of dissolved inorganic carbon in seawater.

In section 13ZS, whether the aforementioned factors have affected the $\delta^{13}C_{carb}$ has been assessed (Zhang et al., 2017). For instance, several traditional methods were used to rule out the possibility of strong diagenetic overprinting. These include microscope and cathodoluminescence examination, Sr and Mn concentrations, Mn/Sr ratios, and $^{87}Sr/^{86}Sr$ ratios. In order to evaluate possible effects of mixed different components, we compared the $\delta^{13}C_{carb}$ data from section 13ZS to the $\delta^{13}C_{carb}$ data from a parallel section (10/11TM) (Fig. 8), and these two sections are situated ~50 m away from each other at Tingri. Similarity of stepped $\delta^{13}C_{carb}$ variations from two sections indicates that the effects of mixed different components on the stepped $\delta^{13}C_{carb}$ record must be insignificant (Fig. 8) (Zhang et al., 2017), further implying that different components in bulk carbonate (mainly micrites and LBF fragments) should have very limited $\delta^{13}C$ variances at Tingri.

Since diagenesis and some local processes can be superimposed upon $\delta^{13}C_{carb}$ records used to track global changes in ocean-atmosphere $\delta^{13}C$ composition (Banner and Hanson, 1990; Patterson and Walter, 1994; Panchuk et al., 2006), one fundamental method to test the validity of the $\delta^{13}C_{carb}$ data is to compare them to the $\delta^{13}C$ data of age-equivalent mixed-layer planktonic foraminifera from pelagic sections that are widely used to monitor changes in the

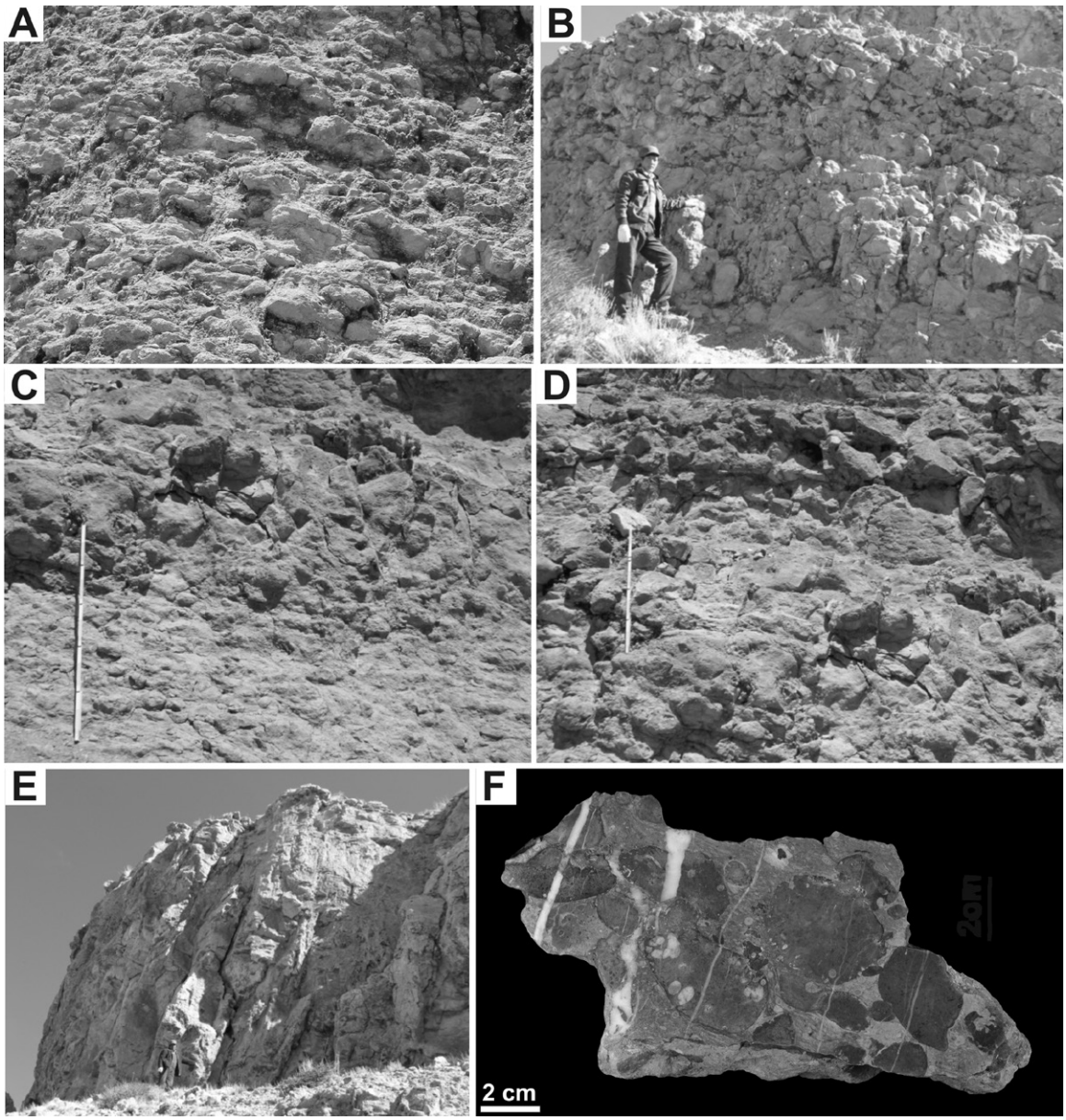

Figure 5. Field photographs (A–E) and a microphotograph from a polished slab of the conglomerate (F) showing carbonate lithologies in sections 13ZS and 11TMG. (A) Nodular limestone recording the main carbon isotope excursion in section 13ZS. (B) Nodular limestone at the base of section 11TMG. (C) The lower part of a lithological unit showing upward changes from nodular marl to nodular limestone in section 11TMG. (D) The upper part of a lithological unit showing upward changes from nodular limestone to thin-bedded limestone in section 11TMG. (E) Thick-bedded *Alveolina* limestone at Gamba. Note that only the basal 2 m of the *Alveolina* limestone is logged in section 11TMG. (F) The conglomerate immediately underlying the *Alveolina* limestone in section 11TMG.

$\delta^{13}C$ of the surface ocean. For section 11TMG, we compare the pre-CIE $\delta^{13}C_{carb}$ values to those of planktonic foraminifer genus *Acarinina* from some pelagic sections (Fig. 4), and the comparison is only focused on the pre-CIE interval because these *Acarinina* $\delta^{13}C$ records might fail to document the full CIE owing to severe carbonate dissolution on pelagic sections (Zachos et al., 2005). In Figure 4, although most $\delta^{13}C_{carb}$ values from section 11TMG (Gamba) are slightly lower than the *Acarinina* $\delta^{13}C$ values from Ocean Drilling Program (ODP) Sites 689 and 690 (paleolatitude ~65 °S), they still fall into the range of the $\delta^{13}C$ variations from ODP Site 527 (paleolatitude ~35°S). The slightly higher $\delta^{13}C$ values at ODP Sites 689 and 690 relative to those at Gamba (paleolatitude ~10°N) may be ascribed to temperature-dependent thermodynamic carbon isotopic fractionation during the air-sea CO_2 exchange, which tends to make the $\delta^{13}C$ values in high latitudinal surface ocean higher than those in equatorial surface ocean (Gruber et al., 1999). Moreover, the ranges of pre-CIE $\delta^{13}C_{carb}$ variations from sections 11TMG and 13ZS are almost identical (Fig. 4), probably indicating that both have recorded the pre-CIE $\delta^{13}C$ fluctuations of local sea water

in the Tibetan Tethyan Ocean. Our previous study showed that there was a close similarity of $\delta^{13}C_{carb}$ curves from two parallel sections (section 13ZS and 10/11TM) at Tingri (Fig. 8) (Zhang et al., 2017), likely indicating that different components in bulk carbonate have very similar $\delta^{13}C$ values. Presumably, "the effect of mixed different components" on the $\delta^{13}C_{carb}$ record in section 11TMG should also be small, because both section 11TMG and section 13ZS are located within the southern Tibetan Himalaya and contain similar biotic components (Figs. 3 and 4). Taken together, we suggest that diagenesis and local factors should have had limited effects on the $\delta^{13}C_{carb}$ records from section 11TMG, and the $\delta^{13}C_{carb}$ record can be used to study carbon perturbations during the PETM.

The CIE Records at Tingri and Gamba

In section 13ZS, the most prominent feature of its $\delta^{13}C_{carb}$ record is that the CIE record is expanded and has a stepped structure (Fig. 3). The stepped CIE structure consists of several distinct phases of $\delta^{13}C_{carb}$ variations (Zhang et al., 2017). In the stepped CIE records, the CIE onset was suggested to have lasted ≤5 k.y. (Farley and Eltgroth, 2003; Röhl et al., 2007; Zeebe et al., 2009). Thus, the P/E boundary in section 13ZS can be pinpointed precisely owing to the presence of the CIE onset in the stepped CIE record (Fig. 8). In section 11TMG, although the expression of the stepped CIE structure is absent, partial records of the pre-CIE, the main CIE, and the CIE recovery can still be recognized (Fig. 8). It implies that the time interval of the latest Paleocene and the earliest Eocene is partly preserved in this section. However, the designation of the P/E boundary in section 11TMG cannot be as precise as that in section 13ZS.

The preservation of the stepped CIE in section 13ZS indicates that the aforementioned factors should have had very limited effects on the $\delta^{13}C_{carb}$ record at Tingri. However, the absence of the stepped CIE in section 11TMG implies that some factors that are not discussed before should have exerted effects on the $\delta^{13}C_{carb}$ record at Gamba. In section 11TMG, the main CIE is recorded in nodular marl and nodular limestone, while in section 13ZS it is preserved in a purely nodular limestone. We cannot ascertain whether the varying lithologies in section 11TMG have affected its $\delta^{13}C_{carb}$ record. But, we tentatively assume that the factor of "reworking" might hinder the preservation of the stepped CIE structure in section 11TMG.

Thin section analysis shows that the dominant LBFs in these two sections are similar during the main CIE interval (Figs. 3 and 4), mainly including the genera *Miscellanea*, *Ranikothalia*, *Lockhartia*, *Kathina*, and *Operculina*, and indicating a paleo-water depth of ~40–80 m (Hottinger, 1997). In section 11TMG, however, the porcellaneous-walled *Alveolina vredenburgi*, a shallow-water dweller, is also moderately frequent, whereas its occurrence in section 13ZS is rather rare. This may imply that the water depth of section 11TMG was probably shallower than that of section 13ZS, although both might still be within ~40–80 m. Modern studies suggest that wave agitation can penetrate into a water depth of ~100 m, and the probability of wave encounter with the sediment-water interface increases significantly as water depth decreases (Peters and Loss, 2012). Presumably, section 11TMG was formed in a slightly shallower depositional environment where carbonate sediments were frequently stirred and locally redistributed so that the stepped CIE structure was disrupted by wave agitation. By contrast, carbonate sediments in section 13ZS might have avoided strong effects of wave agitation by being situated in relatively deeper water, thus preserving a thicker, more complete, less disturbed CIE record.

The P/E Boundary in the Tethyan SBZs

Mainly based on studies of alveolinids and nummulitids from the western Tethyan realm, 20 standard SBZs covering the time span of the Paleocene and Eocene were established by Serra-Kiel et al. (1998) and were later complemented by other authors (Hottinger et al., 1998; Sameeni and Butt, 2004; Hottinger, 2009; Haynes et al., 2010; Zhang et al., 2013; Özcan et al., 2014). The SBZs can be correlated with standard planktonic foraminiferal zones, calcareous nannoplankton zones, and with global magnetic polarity time scale (Serra-Kiel et al., 1998), enabling construction of high-resolution chrono- and biostratigraphy in LBF-bearing carbonate sequences. At Tingri and Gamba, direct correlation of the SBZs to plankton biozonation scheme cannot be confirmed owing to the scarcity of calcareous nannofossils and planktonic foraminifers in the studied sections. By following correlation schemes between SBZs and plankton biozonations proposed by Serra-Kiel et al. (1998) and Papazzoni et al. (2017), the P/E boundary, being situated in the P5b in the planktonic foraminiferal zones and the NP9b in the calcareous nannofossil zones (Dupuis et al., 2003), should fall within the range between the upper SBZ4 and SBZ6.

At Tingri, the LBF assemblages below ~18.4 m in section 13ZS mainly consist of *Miscellanea miscella*, *M. dukhani*, *Ranikothalia nuttalli*, *R. sindensis*, *Lockhartia conditi*, *L. haimei*, *L. hunti*, *L. tipperi*, *Orbitosiphon punjabensis*, *Kathina nammalensis*, *Operculina* sp., *Alveolina* sp., *Setia tibetica*, and *Daviesina langhami*. Immediately above ~18.4 m in the section, the LBF assemblages are composed of *Alveolina subsolanus*, *A. agerensis*, *A. ellipsoidalis*, and *Orbitolites* sp. (Figs. 3 and 6). At Gamba, the LBF assemblages below ~19 m in section 11TMG are composed of *Miscellanea miscella*, *M. dukhani*, *Ranikothalia nuttalli*, *R. savitriae*, *Alveolina vredenburgi*, *Lockhartia conditi*, *L. haimei*, *L. hunti*, *L. tipperi*, *Orbitosiphon punjabensis*, *Kathina nammalensis*, *Operculina* sp., *Setia tibetica*, and *Daviesina langhami*. Above, the LBFs are dominated by *Alveolina subsolanus*, *A. ellipsoidalis*, *Orbitolites* sp., *Nummulites* sp., and *Assilina* sp. (Figs. 4 and 7).

Among all these LBF taxa, *M. miscella*, *R. nuttalli*, *A. vredenburgi*, and *A. ellipsoidalis* have been widely reported from the Tethyan realm, including Tibet, India, and Pakistan in the east to Egypt, Slovenia, and Spain in the west (Hottinger, 1971; Leppig, 1988; Jauhri, 1996, 1998; Hottinger et al., 1998; Hottinger, 2009; Pujalte et al., 2009; Scheibner and Speijer, 2009; Afzal et al., 2010; Zamagni et al., 2012), and their biostratigraphic distribution in the standard

Figure 6 (*on following page*). The latest Paleocene–earliest Eocene larger benthic foraminifera from section 13ZS. A—*Miscellanea miscella* (d'Archiac and Haime 1853), 13ZS47, 10.1 m, SBZ5. B—*Miscellanea miscella* (d'Archiac and Haime 1853), 13ZS52, 11.1 m, SBZ5. C—*Miscellanea dukhani* Smout 1954, 13ZS48, 10.3 m, SBZ5. D—*Ranikothalia sindensis* (Davies 1927), 13ZS57, 12.2 m, SBZ4-SBZ5. E—*Ranikothalia nuttalli* (Davies 1927), 13ZS47, 10.1 m, SBZ5. F—*Ranikothalia nuttalli* (Davies 1927), 13ZS26, 5.8 m, SBZ5. G—*Lockhartia haimei* (Davies 1927), 13ZS09, 2 m, SBZ3-SBZ5. H—*Lockhartia conditi* (Nuttall 1926), 13ZS35, 7.75 m, SBZ5-SBZ8. I—*Lockhartia hunti* Ovey 1947, 13ZS12, 2.4 m, SBZ5-SBZ8. J—*Lockhartia tipperi* (Davies 1926), 13ZS23, 5 m, SBZ5-SBZ8. K—*Setia tibetica* (Douvillé 1916), 13ZS42, 9.1 m, SBZ4-SBZ5. L—*Kathina nammalensis* Smout and Haque 1956, 13ZS43, 9.3 m, SBZ4-SBZ5. M—*Operculina* sp., 13ZS41, 8.9 m, SBZ5-?. N—*Orbitosiphon punjabensis* (Davies 1937), 13ZS38, 8.2 m, SBZ4-SBZ5. O—*Daviesina langhami* Smout 1954, 13ZS13, 2.65 m, SBZ4-SBZ5. P—*Orbitolites* sp., 13ZS99, 21.02 m, SBZ5-?. Q—*Alveolina ellipsoidalis* Schwager 1883, 13ZS93, 19.8 m, SBZ6.

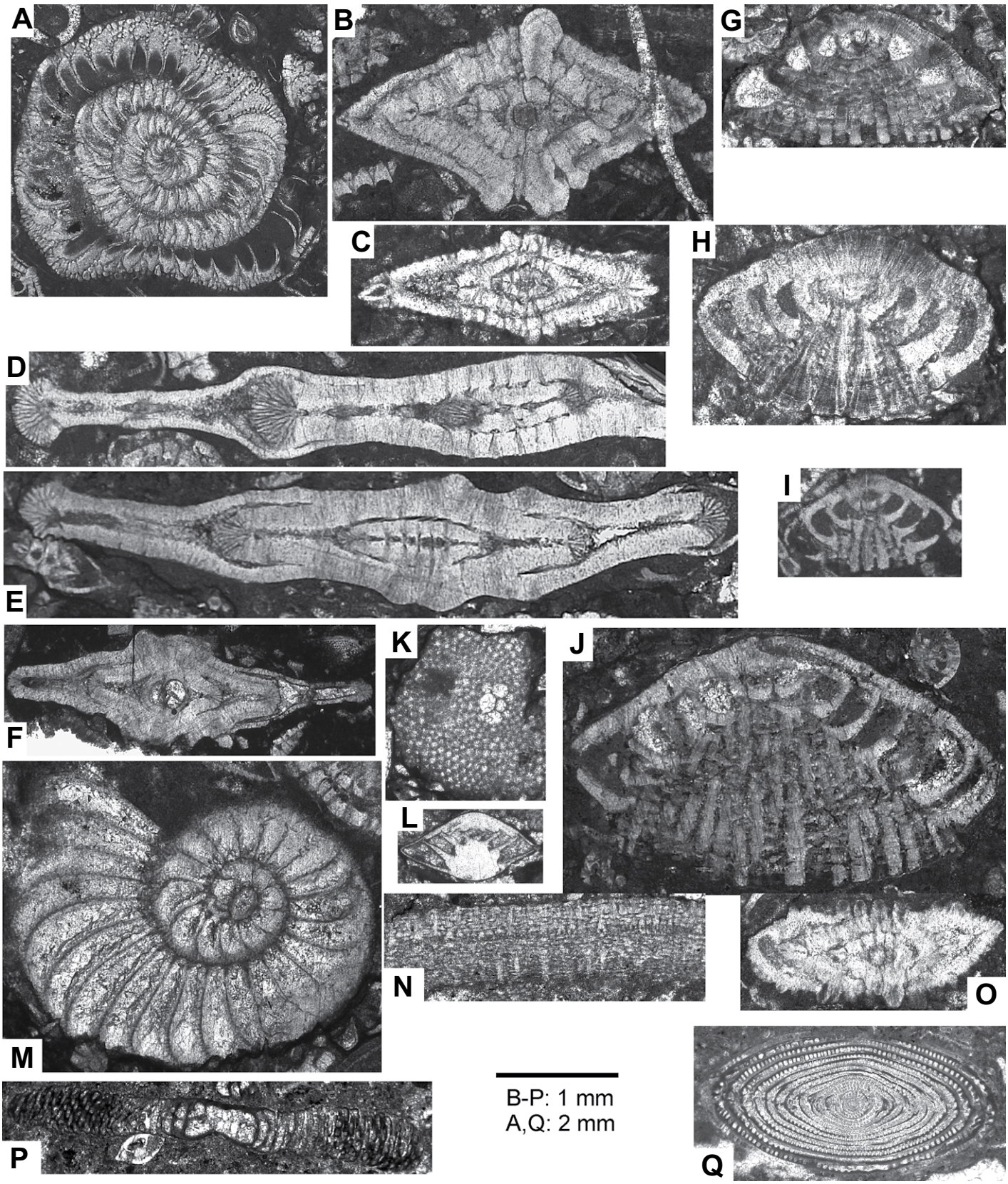

Figure 6.

SBZs is rather clear. *M. miscella* was suggested to occupy two biozones of SBZ4–5, while *R. nuttalli* has a higher stratigraphic position of SBZ5 (Serra-Kiel et al., 1998). In addition, *A. vredenburgi* and *A. ellipsoidalis* are regarded as index fossils for SBZ5 and SBZ6, respectively (Serra-Kiel et al., 1998). In the west, *M. miscella* was found in SBZ4 (Scheibner and Speijer, 2009; Zamagni et al., 2012), whereas in the east it occupies a higher stratigraphic position of SBZ5, as evidenced by its coexistence with *R. nuttalli* and *A. vredenburgi* (Figs. 3 and 4) (Hottinger, 1971; Jauhri, 1998; Hottinger, 2009; Zhang et al., 2013). This coexistence cannot be a result of the local reworking of *M. miscella*, because its abundance in the LBF assemblages is very high and this coexistence was reported from many different locations in the eastern Tethyan realm, such as Tibet, India and, Pakistan (Jauhri, 1998; Afzal et al., 2010; Zhang et al., 2013). Thus, the coexistence of *M. miscella*, *R. nuttalli* and *A. vredenburgi* in Tibet can be taken as an indicator of SBZ5. Based on studies of the major LBF taxa, we suggest that both sections of 13ZS and 11TMG cover stratigraphic intervals of SBZ5 and SBZ6 (Figs. 3 and 4). The SBZ5/SBZ6 transition is situated at ~19 m in section 11TMG and at ~18.4 m in section 13ZS, associated with a sedimentary hiatus in both sections. This sedimentary hiatus was interpreted as reflecting a local tectonic uplift owing to the India-Asia collision (Zhang et al., 2012). Clearly, the P/E boundary, defined as the CIE onset, is located within SBZ5 in the sections (Figs. 3 and 4), not at the SBZ4/SBZ5 transition.

Some previous studies have placed the P/E boundary at the SBZ4/SBZ5 transition. However, the SBZs are chronologically discrete zones. Each biozone is often formed in the context of marine transgression and the neighboring biozones are actually separated by sedimentary hiatuses, not boundaries (Hottinger and Schaub, 1960; Serra-Kiel et al., 1998; Pignatti and Papazzoni, 2017). So, the SBZs differ in principle from continuous plankton-nannoplankton zonations, although they appear to be continuous in the correlation schemes between standard SBZs and other biozonations (Serra-Kiel et al., 1998). Consequently, the P/E boundary may not correspond with the SBZ4/SBZ5 transition in the standard SBZs for inter-biozonal correlation (Serra-Kiel et al., 1998), even though the CIE onset was found to coincide with this transition in the studied sections. For instance, Zamagni et al. (2012) investigated several shallow-marine sections from the Adriatic carbonate platforms and suggested that the P/E boundary was located at the SBZ4/SBZ5 transition. However, frequent occurrence of the porcellaneous-walled *Glomalveolina*, *Lacazina*, and *Alveolina* close to the P/E boundary in these sections might indicate that the water depths was probably less than ~40 m (Hottinger, 1997), shallower than that at Tingri and Gamba. Thus, carbonate sediments in these sections should be more susceptible to wave agitation and highly sensitive to minor sea-level changes, and thus have the lower possibility of preserving an intact CIE record. This inference is supported by the lack of the stepped CIE record from these sections. Moreover, the SBZ4/SBZ5 transition in these sections coincides with sudden changes in the composition of the LBFs, color of the sediments, and microfacies, likely reflecting the existence of a sedimentary hiatus. The existence of a sedimentary hiatus at the SBZ4/SBZ5 transition corresponds with the nature of discrete SBZs. If this sedimentary hiatus reflects time loss of the latest Paleocene and if the missing stratigraphic interval represents the lower SBZ5, the P/E boundary in the sections from the Adriatic carbonate platforms will thus fall within SBZ5, not at the SBZ4/SBZ5 transition.

Response of LBF Assemblages to the PETM

According to the age models constructed for ODP Site 690 (Farley and Eltgroth, 2003; Röhl et al., 2007), the duration of the pre-CIE and the main-CIE is ~30–50 k.y. and ~50–80 k.y., respectively. The similarity in the stepped CIE profiles from the pre-CIE and the main CIE intervals between Tingri and ODP Site 690 probably indicates similar durations of the corresponding phases at Tingri (Fig. 8) (Zhang et al., 2017). Therefore, section 13ZS at Tingri provides a rare opportunity to closely examine changes in LBF assemblages during the time period of ~50 k.y. prior to and after the P/E boundary.

In section 13ZS, the LBF assemblages in the pre-CIE and the main CIE intervals are almost identical, both consisting of *Miscellanea miscella*, *M. dukhani*, *Ranikothalia nuttalli*, *Lockhartia conditi*, *L. haimei*, *L. hunti*, *L. tipperi*, *Orbitosiphon punjabensis*, *Kathina nammalensis*, *Operculina* sp., *Setia tibetica*, *Daviesina langhami*, and *Alveolina* sp. (Figs. 3, 9A, and 9C). At the CIE onset, no evident change in the taxonomic composition of LBF assemblages is observed (Figs. 3, 9A, and 9B). Immediately above the stratigraphic interval of the main CIE, however, a major compositional change in LBF assemblages occurs, characterized by the sudden disappearance of *Miscellanea*, *Lockhartia*, *Ranikothalia*, *Operculina*, *Kathina*, *Setia*, *Daviesina*, *Orbitosiphon* and the initial dominance of porcellaneous-walled *Alveolina* and *Orbitolites* together with abundant small miliolids and rotaliids (Figs. 3, 9C, and 9D). The term "larger foraminiferal extinction and origination" (LFEO) was coined to describe this change in LBF assemblages (Zhang et al., 2013). Subsequently, small miliolids and rotaliids disappeared quickly. During the early Eocene, the LBF assemblages, mainly consisting of *Alveolina-Orbitolites*, *Alveolina-Nummulites*, and *Discocyclina-Assilina-Nummulites*, dominated the carbonate ramp sequentially, as depositional environments of these sections changed gradually from inner ramp, mid-ramp, to outer ramp before the carbonate ramp was drowned ~52 m.y. ago (Zhang et al., 2012). During this period, *Miscellanea*, *Ranikothalia*, *Setia*, and *Orbitosiphon* were extinct. Most *Lockhartia* species also disappeared, and only a few of them can be occasionally found in the Eocene strata, but with reduced shell sizes and abundance (Zhang et al., 2013; Kahsnitz et al., 2016).

At Gamba, similar stratigraphic variations in LBF assemblages can be found in section 11TMG and other sections investigated by Li et al. (2017), showing no compositional change in LBF assemblages at the P/E boundary and the occurrence of the LFEO immediately above the main CIE interval (Fig. 4). Both at Tingri and Gamba, the LFEO occurs within the CIE recovery (Figs. 3 and 4), which has been esti-

Figure 7 (*on following page*). The latest Paleocene–earliest Eocene larger benthic foraminifera from section 11TMG. A—*Miscellanea miscella* (d'Archiac and Haime 1853), 11TMG23, 4.8 m, SBZ5. B—*Miscellanea dukhani* Smout 1954, 11TMG2, 0.3 m, SBZ5. C—*Ranikothalia nuttalli* (Davies 1927), 11TMG2, 0.3 m, SBZ5. D–E—*Alveolina vredenburgi* Davies and Pinfold 1937, 11TMG54, 12 m, SBZ5. F—*Lockhartia hunti* Ovey 1947, 11TMG92, 17.7 m, SBZ5-SBZ8. G—*Lockhartia conditi* (Nuttall 1926), 11TMG68, 14.25 m, SBZ5-SBZ8. H—*Lockhartia haimei* (Davies 1927), 11TMG6, 1.15 m, SBZ3-SBZ5. I—*Lockhartia tipperi* (Davies 1926), 11TMG100, 19.15 m, SBZ5-SBZ8. J—*Orbitosiphon punjabensis* (Davies 1937), 11TMG8, 1.65 m, SBZ4-SBZ5. K—*Kathina nammalensis* Smout and Haque 1956, 11TMG97, 18.8 m, SBZ4-SBZ5. L—*Daviesina langhami* Smout 1954, 11TMG91, 17.55 m, SBZ4-SBZ5. M—*Assilina* sp., 11TMG99, 19.05 m, SBZ6-?. N—*Alveolina subsolanus* (Sheng and Zhang 1976), 11TMG101, 19.45 m, SBZ6-?. O—*Alveolina ellipsoidalis* Schwager 1883, 11TMG102, 19.7 m, SBZ6. P—*Nummulites* sp., 11TMG99, 19.05 m, SBZ6-?.

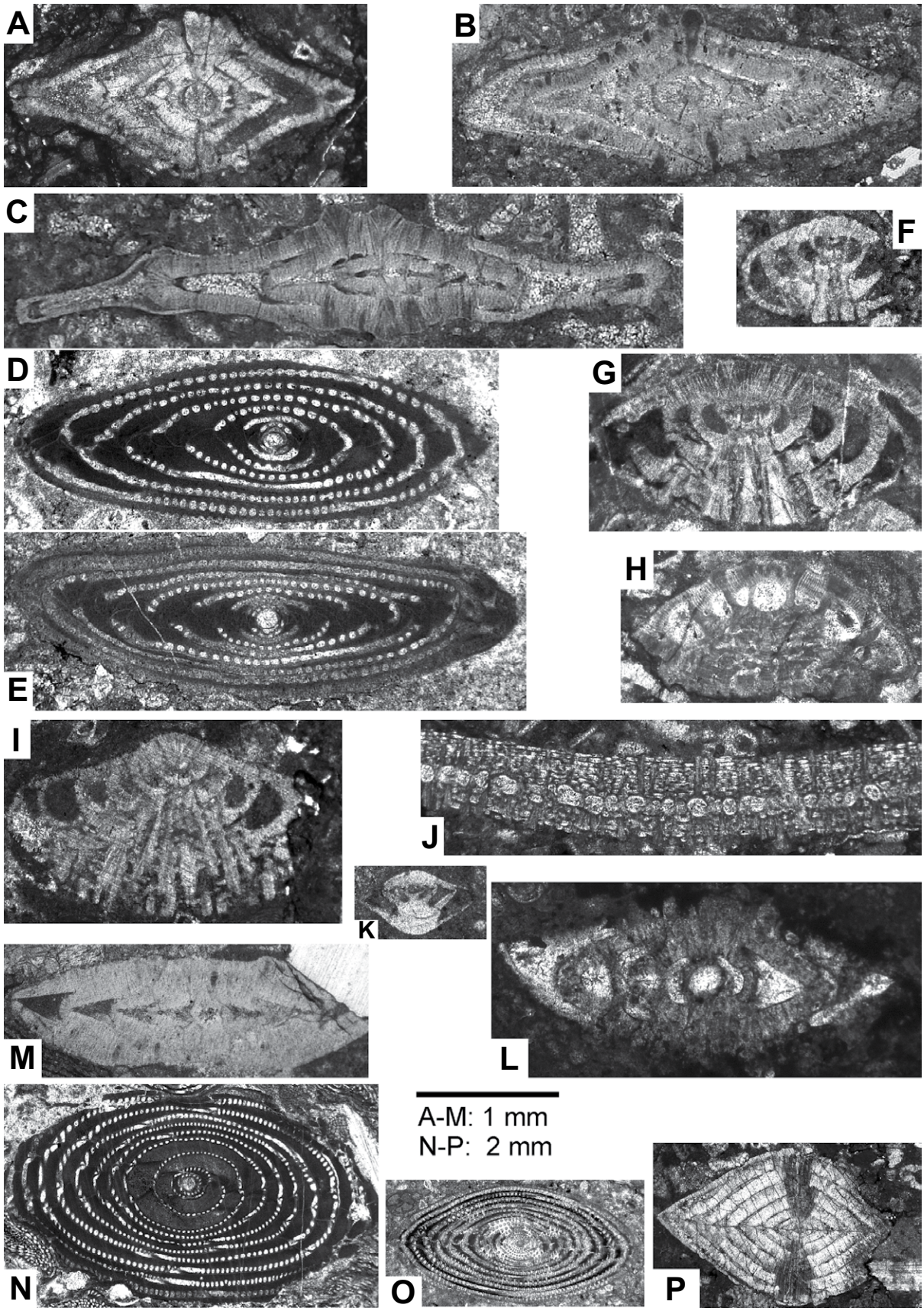

Figure 7.

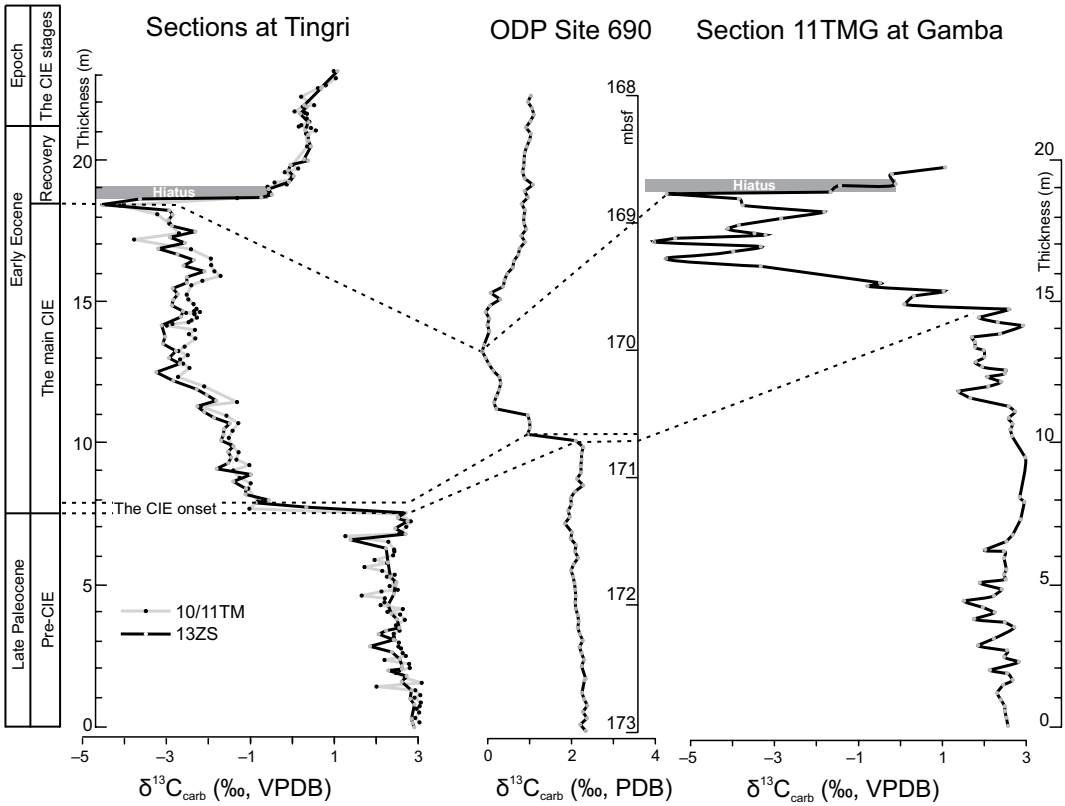

Figure 8. Comparison of the carbon isotope excursion (CIE) structure among Tingri, ODP Site 690 and Gamba. Note that the CIE records from two parallel sections at Tingri (section 13ZS and section 10/11TM) can reproduce the stepped CIE structure, and this stepped CIE structure is very similar to that at ODP Site 690. The carbon isotope record at Ocean Drilling Program (ODP) Site 690 is taken from Bains et al. (1999), and two CIE records at Tingri are from Zhang et al. (2017). mbsf—meter below sea floor.

mated to have lasted ~30–120 k.y. (Farley and Eltgroth, 2003; Röhl et al., 2007). Thus, the LFEO should have taken place rapidly in this short time period.

In sections 13ZS and 11TMG, the LFEO coincides with the SBZ5/SBZ6 transition and with a sedimentary hiatus that is marked by the presence of a conglomerate layer in section 11TMG and selective meteoric diagenesis in section 13ZS (Zhang et al., 2017). The existence of the sedimentary hiatus hinders a tight stratigraphic constraint on the LFEO so that the occurrence of the LFEO can only be placed within the stratigraphic interval between the upper SBZ5 and the lower SBZ6 in the standard SBZs for inter-biozonal correlations (Serra-Kiel et al., 1998). In Pakistan, similar compositional changes in LBF assemblages was also reported to have happened within the combined biozones of SBZ5/SBZ6 (Afzal, et al., 2010), which is consistent with this study in south Tibet.

In Egypt, a compositional change in LBF assemblages was observed, but its occurrence was thought to be at SBZ4/SBZ5 transition (Scheibner and Speijer, 2009). In their suggested SBZ4, however, *Ranikothalia nuttalli*, a typical SBZ5 species (Serra-Kiel, et al., 1998), appears together with some index fossils of SBZ4 (e.g., *Hottingerina lukasi*, *Glomalveolina levis*). Above this biozone, two combinational zones of SBZ5/SBZ6 were assigned, owing to the coexistence of *Alveolina vredenburgi* (an index fossil of SBZ5) and *Alveolina ellipsoidalis* (an index fossil of SBZ6) as well as other LBF taxa (e.g., *Nummulites*, *Orbitolites*, and *Cuvillierina*) (Scheibner and Speijer, 2009). The studied sections with relatively clear CIE records were mainly formed in the lower slope, toe of slope, and deep basin (Scheibner and Speijer, 2009), and the co-occurrence of LBF taxa from different SBZs is probably a result of sediment reworking, as evidenced by the presence of slump and debris flow in these sections (Scheibner and Speijer, 2009). In this case, the designation of SBZs should be based on the youngest species in the mixed LBF assemblages, and the suggested SBZ4 and combined SBZ5/SBZ6 may be interpreted as SBZ5 and SBZ6, respectively. Thus, this major LBF change in Egypt would occur at the SBZ5/SBZ6 transition, not at the SBZ4/SBZ5 transition as suggested before (Scheibner and Speijer, 2009).

The major LBF change in Egypt was referred to as the "larger foraminiferal turnover" (LFT) (Scheibner and Speijer, 2009), because the LFT was formerly proposed to occur across the SBZ4/SBZ5 transition where *Alveolina* started to show dimorphism and to have larger shell sizes (Hottinger, 1998). For some other Paleocene LBFs, however, they started to show dimorphism in SBZ3, such as *Miscellanites primitivus*, *Miscellanites minutus*, *Miscellanites iranicus*, *Miscellanea juliettae*, *Miscellanea yvettae*, *Keramosphaerinopsis haydeni*, and *Nummulites heberti* (Leppig, 1988; Racey, 1995; Serra-Kiel et al., 1998; Cherchi and Schroeder, 2005; Hottinger, 2009; Zhang et al., 2013). We therefore tentatively suggest the concept of the LFT might be only suitable for investigating species-level evolution within a certain genus, because different LBF genera experienced their LFT at different times. Although the LFT within the genus *Alveolina* happened at the SBZ4/SBZ5 transition, it may be inappropriate to assert that all LBF taxa have experienced their LFT at the SBZ4/SBZ5 transition simultaneously.

Investigations of orthophragminids (LBF) from the same sections in Egypt have called into question the proposal linking this major compositional change in LBF taxa to the LFT (Özcan et al., 2014), and this LBF change in Egypt seems similar to the LFEO from Tibet and Pakistan, both reflecting a sudden extinction of some Paleocene LBFs that once thrived in the Tethyan Ocean. The LFEO event does not reflect a local facies change, because it likely happens over a wide area of the Tethyan realm and leads to an extinction of some major Paleocene LBFs. Also, this event does not reflect the evolutionary suc-

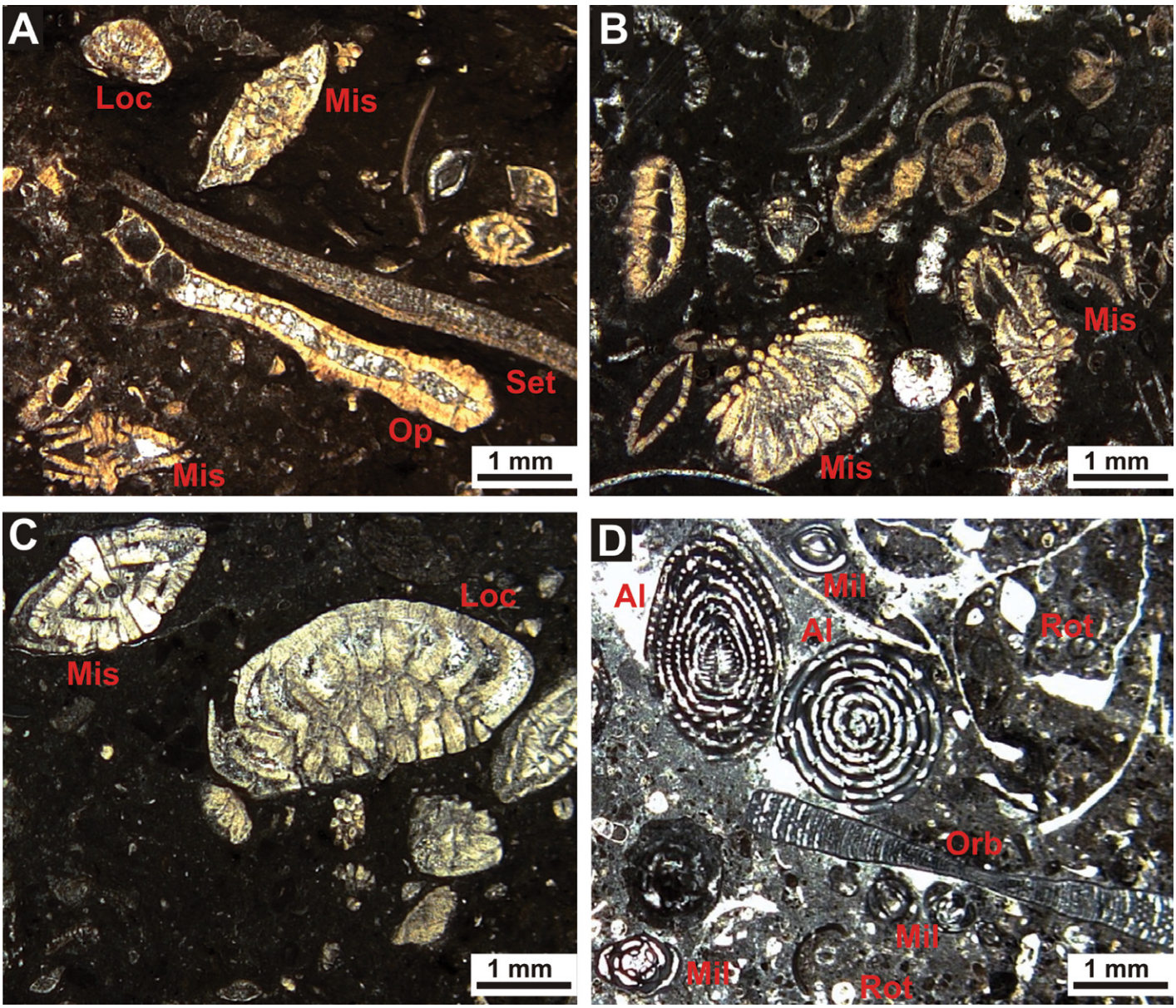

Figure 9. Thin-section photomicrographs showing compositional changes in larger benthic foraminifer (LBF) assemblages during the Paleocene-Eocene thermal maximum. As shown in (A), (B) and (C), there is no compositional change in LBF assemblages at the carbon isotope excursion (CIE) onset and in the main CIE interval. Instead, a major compositional change in the LBF assemblages occurs in the CIE recovery (D). Stratigraphic positions of these photomicrographs can be found in Figure 3. Abbreviations: Al—*Alveolina*; Loc—*Lockhartia*; Mil—small miliolids; Mis—*Miscellanea*; Op—*Operculina*; Orb—*Orbitolites*; Rot—small rotaliids; Set—*Setia*.

cess of K-strategist LBFs as proposed by Hottinger (1998). Instead, the LFEO may represent a response of the LBFs to the drastic environmental perturbation during the PETM.

Across the CIE onset, a large amount of ^{13}C-depleted carbon was released into the atmosphere-ocean system, causing a pronounced negative CIE and severe carbonate dissolution on the deep-sea floor (McInerney and Wing, 2011; Zachos et al., 2005). In the CIE recovery, however, the $\delta^{13}C$ values in exogenic carbon pools increased gradually, implying that some negative feedback mechanisms commenced and the released carbon was progressively removed from the ocean-atmosphere system. Although the mechanisms causing the carbon removal are still debated, different lines of evidence imply that intensified continental weathering should have played an important role in arresting PETM conditions (Kelly et al., 2005, 2010; Chen, et al., 2016; Penman, 2016). Intensified continental weathering, likely related to a rise of atmospheric pCO_2 and acceleration of hydrological cycling (Pagani et al., 2006), would increase nutrient input to coastal waters where LBFs are usually found. Most LBF taxa harbor photosymbiotic algae (Leutenegger, 1984), and the maintenance of the host-symbiont relationship is of benefit to both the LBFs and algae (Hallock, 2000). The growth of symbiotic algae in LBFs requires sufficient light level and a minimum temperature of ~16–18 °C (Hollaus and Hottinger, 1997). During the PETM, sea-surface

temperature started to increase from the pre-CIE interval (Sluijs et al., 2007), and probably reached to the maximum in the main CIE interval (Nicolo et al., 2010). It was suggested that the temperature in the main CIE interval was >40 °C in the tropical surface ocean (Aze et al., 2014) and high temperature might had persisted >20 k.y. after the $\delta^{13}C$ minimum, into the early CIE recovery (Nicolo et al., 2010). Thus, sea surface temperature during the CIE recovery at Tingri and Gamba was very unlikely below the minimum temperature for the growth of symbiotic algae. However, if the temperature was extremely high at that time, it may lead to the occurrence of the LFEO by breaching temperature tolerance thresholds of the LBFs, as suggested for the PETM planktonic foraminifer in Tanzania (Aze et al., 2014). Unfortunately, the lack of good constraints on the temporal changes in the PETM temperature from south Tibet hinders further understanding of the temperature's role on the LBF evolution.

With respect to light availability, increased nutrient input into the ocean can reduce water transparency and cause eutrophication and plankton blooming, leading to a deficiency of light availability in the water column. Insufficient light may further impede the photosynthetic activity of symbiotic algae and lead to the breakdown of photosymbiosis among LBF taxa. The inference of increased nutrient input is indirectly supported by the appearance of small miliolids and rotaliids within the CIE recovery interval as they are herbivorous and detritivorous taxa (Hallock, 2000). We therefore speculate that the LFEO during the CIE recovery might be related to a transient episode of eutrophication in shallow neritic waters, and that the eutrophication may have been caused by intensified continental weathering.

CONCLUSIONS

We measured the $\delta^{13}C_{carb}$ of bulk carbonate and studied larger benthic foraminiferal (LBFs) assemblages from two shallow-marine carbonate sections in south Tibet that cover the key interval of the PETM. Evaluations on the $\delta^{13}C_{carb}$ data suggested that diagenesis and local factors had limited effects on the $\delta^{13}C_{carb}$ records from these two sections. Comparison of the detailed $\delta^{13}C_{carb}$ variations among the sections from Tingri, Gamba, and ODP Site 690 indicated that the stratigraphic interval of the uppermost Paleocene-lowermost Eocene was well preserved in the sections from south Tibet, particularly in section 13ZS at Tingri. The clear expression of the CIE onset in section 13ZS allows us to pinpoint the P/E boundary precisely in this eastern Tethyan section.

Two shallow benthic zones (SBZs) were recognized within the sections, SBZ5 and SBZ6. The combined evidence of the $\delta^{13}C_{carb}$ records and the SBZ biostratigraphy clearly shows that the P/E boundary is situated within SBZ5, not at the SBZ4/SBZ5 transition as proposed from some western Tethyan sections. However, we cannot rule out the possibility that the LBF datums marking SBZ4 and SBZ5 are diachronous in the Tethyan Ocean, and future investigations of the upper Paleocene–lower Eocene LBF-rich sections from other Tethyan regions containing calcareous plankton is needed to further clarify this issue and confirm the interpretations herein reported.

A close examination of the LBF assemblages in the sections suggests that there is no evident change in the taxonomic composition of the LBF assemblages across the CIE onset. However, a "larger foraminiferal extinction and origination" (LFEO) event took place during the CIE recovery, characterized by the sudden disappearance of *Miscellanea*, *Lockhartia*, *Ranikothalia*, *Operculina*, *Kathina*, *Setia*, *Orbitosiphon* and the initial dominance of porcellaneous-walled *Alveolina* and *Orbitolites* together with small miliolids and rotaliids. The LFEO differs from the traditional "larger foraminiferal turnover" event in that it reflects a sudden extinction event in the LBF community, likely related to increased continental weathering and resultant eutrophication in the Tethyan Ocean during the recovery phase of the PETM. Whether the LFEO, as defined in this study, occurred synchronously throughout the entire Tethyan Ocean region remains unclear.

ACKNOWLEDGMENTS

We thank A. Hübner and C. Schott for the preparation of rock thin sections, and M. Segl for technical help in the laboratories. Funding for this research was provided by the National Key Research and Development Plan (2016YFC0600303), National Natural Science Foundation of China (41490615), the Deutsche Forschungsgemeinschaft (No. Wi725/29), and CAS Pioneer Hundred Talents Program. Clay Kelly (the associate editor), Johannes Pignatti, and an anonymous reviewer are thanked for their detailed comments that improved the quality of this paper significantly.

REFERENCES CITED

Afzal, J., Williams, M., Leng, M.J., Aldridge, R.J., and Stephenson, M.H., 2010, Evolution of Paleocene to Early Eocene larger benthic foraminifer assemblages of the Indus Basin, Pakistan: Lethaia, v. 44, p. 1–20, 10.1111/j.1502-3931.2010.00247.x.

Archer, D., 2010, How it went down last time: Nature Geoscience, v. 3, p. 819–820, https://doi.org/10.1038/ngeo1031.

Aubry, M.P., and Ouda, K., 2003, Introduction to the upper Paleocene–lower Eocene of the upper Nile Valley: Micropaleontology, v. 49, p. 2–4.

Aze, T., Pearson, P.N., Dickson, A.J., Badger, M.P.S., Bown, P.R., Pancost, R.D., Gibbs, S.J., Huber, B.T., Leng, M.J., Coe, A.L., Cohen, A.S., and Foster, G.L., 2014, Extreme warming of tropical waters during the Paleocene-Eocene Thermal Maximum: Geology, v. 42, p. 739–742, 10.1130/g35637.1.

Bains, S., Corfield, R.M., and Norris, R.D., 1999, Mechanisms of climate warming at the end of the Paleocene: Science, v. 285, p. 724–727, https://doi.org/10.1126/science.285.5428.724.

Banner, J.L., and Hanson, G.N., 1990, Calculation of simultaneous isotopic and trace element variations during water-rock interaction with applications to carbonate diagenesis: Geochimica et Cosmochimica Acta, v. 54, p. 3123–3137, https://doi.org/10.1016/0016-7037(90)90128-8.

Bowen, G.J., Clyde, W.C., Koch, P.L., Ting, S., Alroy, J., Tsubamoto, T., and Wang, Y., 2002, Mammalian dispersal at the Paleocene/Eocene boundary: Science, v. 295, p. 2062–2065, https://doi.org/10.1126/science.1068700.

Chen, Z., Ding, Z., Yang, S., Zhang, C., and Wang, X., 2016, Increased precipitation and weathering across the Paleocene-Eocene Thermal Maximum in central China: Geochemistry Geophysics Geosystems, v. 17, p. 2286–2297, https://doi.org/10.1002/2016GC006333.

Cherchi, A., and Schroeder, R., 2005, Revision of *Keramosphaerinopsis haydeni* (H. Douvillé), larger foraminifer (Miliolacea) from the Paleocene of southern Tibet (Tethys Himalaya): Bollettino della Società Paleontologica Italiana, v. 44, p. 175–183.

Currano, E.D., Wilf, P., Wing, S.L., Labandeira, C.C., Lovelock, E.C., and Royer, D.L., 2008, Sharply increased insect herbivory during the Paleocene-Eocene Thermal Maximum: Proceedings of the National Academy of Sciences of the United States of America, v. 105, p. 1960–1964, https://doi.org/10.1073/pnas.0708646105.

Dickens, G.R., O'Neil, J.R., Rea, D.K., and Owen, R.M., 1995, Dissociation of oceanic methane hydrate as a cause of the carbon isotope excursion at the end of the Paleocene: Paleoceanography, v. 10, p. 965–971, https://doi.org/10.1029/95PA02087.

Ding, L., Kapp, P., and Wan, X., 2005, Paleocene-Eocene record of ophiolite obduction and initial India-Asia collision, south central Tibet: Tectonics, v. 24, p. 1–18, https://doi.org/10.1029/2004TC001729.

Dunkley Jones, T., Lunt, D.J., Schmidt, D.N., Ridgwell, A., Sluijs, A., Valdes, P.J., and Maslin, M., 2013, Climate model and proxy data constraints on ocean warming across the Paleocene-Eocene Thermal Maximum: Earth-Science Reviews, v. 125, p. 123–145, https://doi.org/10.1016/j.earscirev.2013.07.004.

Dupuis, C., Aubry, M.-P., Steurbaut, E., Berggren, W.A., Ouda, K., Magioncalda, R., Cramer, B.S., Kent, D.V., Speijer, R.P., and Heilmann-Clausen, C., 2003, The Dababiya Quarry section: Lithostratigraphy, clay mineralogy, geochemistry and paleontology: Micropaleontology, v. 49, p. 41–59, https://doi.org/10.2113/49.Suppl_1.41.

Farley, K.A., and Eltgroth, S.F., 2003, An alternative age model for the Paleocene-Eocene thermal maximum using extraterrestrial ^{3}He: Earth and Planetary Science Letters, v. 208, p. 135–148, https://doi.org/10.1016/S0012-821X(03)00017-7.

Gibbs, S.J., Bown, P.R., Sessa, J.A., Bralower, T.J., and Wilson, P.A., 2006, Nannoplankton extinction and origination across the Paleocene-Eocene thermal maximum: Science, v. 314, p. 1770–1773, https://doi.org/10.1126/science.1133902.

Gruber, N., Keeling, C.D., Bacastow, R.B., Guenther, P.R., Lueker, T.J., Wahlen, M., Meijer, H.A.J., Mook, W.G., and Stocker, T.F., 1999, Spatiotemporal patterns of carbon-13 in the global surface oceans and the oceanic Suess effect: Global Biogeochemical Cycles, v. 13, p. 307–335, https://doi.org/10.1029/1999GB900019.

Haynes, J.R., Racey, A., and Whittaker, J.E., 2010, A revision of the Early Palaeogene nummulitids (Foraminifera) from northern Oman, with implications for their classification, *in* Whittaker, J.E., and Hart, M.B., eds., Micropalaeontology, Sedimentary Environments and Stratigraphy: A Tribute to Dennis Curry (1912–2001), The Micropalaeontological Society, Special Publications, p. 29–89.

Hallock, P., 2000, Symbiont-bearing foraminifera: Harbingers of global change?: Micropaleontology, v. 46, p. 95–104.

Hollaus, S., and Hottinger, L., 1997, Temperature dependence of endosymbiotic relationships? Evidence from the depth range of Mediterranean *Amphistegina lessonii* (Foraminifera): Eclogae Geologicae Helvetiae, v. 90, p. 591–597.

Hottinger, L., 1971, Larger foraminifera common to Mediterranean and Indian Paleocene and Eocene formations: Annales Instituti Geologici Publici Hungarici, v. 54, p. 145–151.

Hottinger, L., 1997, Shallow benthic foraminiferal assemblages as signals for depth of their deposition and their limitations: Bulletin de la Société Géologique de France, v. 168, p. 491–505.

Hottinger, L., 1998, Shallow benthic foraminifera at the Paleocene-Eocene boundary: Strata, v. 9, p. 61–64.

Hottinger, L., 2001, Learning from the past, *in* Levi-Montalcini, R., ed., Frontiers of life, Volume 4: London & San Diego, Academic Press, p. 449–477.

Hottinger, L., 2009, The Paleocene and earliest Eocene foraminiferal family Miscellaneidae: neither nummulitids nor rotaliids: Carnets de Géologie, v. 6, p. 1–41.

Hottinger, L., and Schaub, H., 1960, Zur Stufeneinteilung des Paleocaens und des Eocaens. Einführung der Stufen Ilerdien und Biarritzien: Eclogae Geologicae Helvetiae, v. 53, p. 453–479.

Hottinger, L., Smeeni, S.J., and Butt, A.A., 1998, Emendation of *Alveolina vredenburgi* Davies and Pinfold, 1937 from the Surghar range, Pakistan, *in* Hottinger, L., and Drobne, K., eds., Paleogene shallow benthos of the Tethys, Volume 34: Ljubljana, Slovenian Academy of Sciences and Arts, p. 155–163.

Immenhauser, A., Holmden, C., and Patterson, W.P., 2008, Interpreting the carbon-isotope record of ancient shallow epeiric seas: Lessons from the recent, *in* Pratt, B.R., and Holmden, C., eds., Dynamics of Epeiric Seas, Volume 48: Geological Association of Canada, p. 137–174.

Jauhri, A.K., 1996, *Ranikothalia nuttalli* (Davies), a distinctive early Ilerdian marker, in the Shillong Plateau, *in* Pandey, J., Azmi, R.J., Bhandari, A., and Dave, A., eds., Contributions to XV Indian Colloquium on Micropalaeontology and stratigraphy: Dehra Dun, Allied Printer, p. 209–218.

Jauhri, A.K., 1998, *Miscellanea* Pfender, 1935 (foraminiferida) from the south shillong region, N.E. India: Journal of the Palaeontological Society of India, v. 43, p. 73–83.

Kahsnitz, M.M., Zhang, Q., and Willems, H., 2016, Stratigraphic distribution of the larger benthic foraminifera *Lockhartia* in south Tibet (China): Journal of Foraminiferal Research, v. 46, p. 34–47, https://doi.org/10.2113/gsjfr.46.1.34.

Kelly, D.C., Bralower, T.J., Zachos, J.C., Premoli-Silva, I., and Thomas, E., 1996, Rapid diversification of planktonic foraminifera in the tropical Pacific (ODP Site 865) during the late Paleocene thermal maximum: Geology, v. 24, p. 423–426, https://doi.org/10.1130/0091-7613(1996)024<0423:RDOPFI>2.3.CO;2.

Kelly, D.C., Zachos, J.C., Bralower, T.J., and Schellenberg, S.A., 2005, Enhanced terrestrial weathering/runoff and surface ocean carbonate production during the recovery stages of the Paleocene-Eocene thermal maximum: Paleoceanography, v. 20, https://doi.org/10.1029/2005PA001163.

Kelly, D.C., Nielsen, T.M.J., McCarren, H.K., Zachos, J.C., and Röhl, U., 2010, Spatiotemporal patterns of carbonate sedimentation in the South Atlantic: Implications for carbon cycling during the Paleocene-Eocene thermal maximum: Palaeogeography, Palaeoclimatology, Palaeoecology, v. 293, p. 30–40, https://doi.org/10.1016/j.palaeo.2010.04.027.

Leppig, U., 1988, Structural analysis and taxonomic revision of *Miscellanea*, Paleocene, larger Foraminifera: Eclogae Geologicae Helvetiae, v. 81, p. 689–721.

Leutenegger, S., 1984, Symbiosis in benthic foraminifera; specificity and host adaptations: Journal of Foraminiferal Research, v. 14, p. 16–35, https://doi.org/10.2113/gsjfr.14.1.16.

Li, J., Hu, X., Garzanti, E., and BouDagher-Fadel, M., 2017, Shallow-water carbonate responses to the Paleocene-Eocene thermal maximum in the Tethyan Himalaya (southern Tibet): Tectonic and climatic implications: Palaeogeography, Palaeoclimatology, Palaeoecology, v. 466, p. 153–165, https://doi.org/10.1016/j.palaeo.2016.11.026.

McInerney, F.A., and Wing, S.L., 2011, The Paleocene-Eocene thermal maximum: A perturbation of carbon cycle, climate, and biosphere with implications for the future: Annual Review of Earth and Planetary Sciences, v. 39, p. 489–516, https://doi.org/10.1146/annurev-earth-040610-133431.

Nicolo, M.J., Dickens, G.R., and Hollis, C.J., 2010, South Pacific intermediate water oxygen depletion at the onset of the Paleocene-Eocene thermal maximum as depicted in New Zealand margin sections: Paleoceanography, v. 25, https://doi.org/10.1029/2009PA001904.

Orue-Etxebarria, X., Pujalte, V., Bernaola, G., Apellaniz, E., Baceta, J.I., Payros, A., Nunez-Betelu, K., Serra-Kiel, J., and Tosquella, J., 2001, Did the Late Paleocene thermal maximum affect the evolution of larger foraminifers? Evidence from calcareous plankton of the Campo Section (Pyrenees, Spain): Marine Micropaleontology, v. 41, p. 45–71, https://doi.org/10.1016/S0377-8398(00)00052-9.

Özcan, E., Scheibner, C., and Boukhalfa, K., 2014, Orthophragminids (foraminifera) across the Paleocene-Eocene transition from North Africa: Taxonomy, biostratigraphy, and paleobiogeographic implications: Journal of Foraminiferal Research, v. 44, p. 203–229, https://doi.org/10.2113/gsjfr.44.3.203.

Pagani, M., Pedentchouk, N., Huber, M., Sluijs, A., Schouten, S., Brinkhuis, H., Sinninghe Damsté, J.S., and Dickens, G.R., and the Expedition 302 Scientists, 2006, Arctic hydrology during global warming at the Palaeocene/Eocene thermal maximum: Nature, v. 442, p. 671–675, 10.1038/nature05043.

Panchuk, K.M., Holmden, C.E., and Leslie, S.A., 2006, Local controls on carbon cycling in the Ordovician mid-continent region of North America, with implications for carbon isotope secular curves: Journal of Sedimentary Research, v. 76, p. 200–211, https://doi.org/10.2110/jsr.2006.017.

Papazzoni, C.A., Ćosović, V., Briguglio, A., and Drobne, K., 2017, Towards a calibrated larger foraminifera biostratigraphic zonation: Celebrating 18 years of the application of shallow benthic zones: Palaios, v. 32, p. 1–5, https://doi.org/10.2110/palo.2016.043.

Patterson, W.P., and Walter, L.M., 1994, Depletion of ^{13}C in seawater ΣCO_2 on modern carbonate platforms: Significance for the carbon isotopic record of carbonates: Geology, v. 22, p. 885–888, https://doi.org/10.1130/0091-7613(1994)022<0885:DOCISC>2.3.CO;2.

Penman, D.E., 2016, Silicate weathering and North Atlantic silica burial during the Paleocene-Eocene Thermal Maximum: Geology, v. 44, p. 731–734, https://doi.org/10.1130/G37704.1.

Peters, S.E., and Loss, D.P., 2012, Storm and fair-weather wave base: A relevant distinction?: Geology, v. 40, p. 511–514, https://doi.org/10.1130/G32791.1.

Pignatti, J., and Papazzoni, C.A., 2017, Oppelzones and their heritage in current larger foraminiferal biostratigraphy: Lethaia, v. 50, p. 369–380, https://doi.org/10.1111/let.12210.

Pujalte, V., Schmitz, B., Baceta, J.I., Orue-Etxebarria, X., Bernaola, G., Dinarès-Turell, J., Payros, A., Apellaniz, E., and Caballero, F., 2009, Correlation of the Thanetian-Ilerdian turnover of larger foraminifera and the Paleocene-Eocene thermal maximum: confirming evidence from the Campo area (Pyrenees, Spain): Geologica Acta, v. 7, p. 161–175, 10.1344/105.000000276.

Racey, A., 1995, Lithostratigraphy and larger foraminiferal (Nummulitid) biostratigraphy of the Tertiary of northern Oman: Micropaleontology, v. 41, p. 1–123, https://doi.org/10.2307/1485849.

Röhl, U., Westerhold, T., Bralower, T.J., and Zachos, J.C., 2007, On the duration of the Paleocene-Eocene thermal maximum (PETM): Geochemistry Geophysics Geosystems, v. 8, p. 1–13, https://doi.org/10.1029/2007GC001784.

Sameeni, S.J., and Butt, A.A., 2004, Alveolinid biostratigraphy of the Salt Range succession, Northern Pakistan: Revue de Paléobiologie, v. 23, p. 505–527.

Scheibner, C., and Speijer, R.P., 2008, Late Paleocene-early Eocene Tethyan carbonate platform evolution—A response to long- and short- term paleoclimatic change: Earth-Science Reviews, v. 90, p. 71–102, https://doi.org/10.1016/j.earscirev.2008.07.002.

Scheibner, C., and Speijer, R.P., 2009, Recalibration of the Tethyan shallow-benthic zonation across the Paleocene-Eocene boundary: Geologica Acta, v. 7, p. 195–214, 10.1344/105.000000267.

Scheibner, C., Speijer, R.P., and Marzouk, A.M., 2005, Turnover of larger foraminifera during the Paleocene-Eocene Thermal Maximum and paleoclimatic control on the evolution of platform ecosystems: Geology, v. 33, p. 493–496, https://doi.org/10.1130/G21237.1.

Schmitz, B., and Pujalte, V., 2007, Abrupt increase in seasonal extreme precipitation at the Paleocene-Eocene boundary: Geology, v. 35, p. 215–218, https://doi.org/10.1130/G23261A.1.

Secord, R., Bloch, J.I., Chester, S.G.B., Boyer, D.M., Wood, A.R., Wing, S.L., Kraus, M.J., McInerney, F.A., and Krigbaum, J., 2012, Evolution of the earliest horses driven by climate change in the Paleocene-Eocene thermal maximum: Science, v. 335, p. 959–962, https://doi.org/10.1126/science.1213859.

Serra-Kiel, J., Hottinger, L., Caus, E., Drobne, K., Ferrandez, C., Jauhri, A.K., Less, G., Pavlovec, R., Pignatti, J., and Samso, J.M., 1998, Larger foraminiferal biostratigraphy of the Tethyan Paleocene and Eocene: Bulletin de la Société Géologique de France, v. 169, p. 281–299.

Sluijs, A., and Dickens, G.R., 2012, Assessing offsets between the $\delta^{13}C$ of sedimentary components and the global exogenic carbon pool across early Paleogene carbon cycle perturbations: Global Biogeochemical Cycles, v. 26, https://doi.org/10.1029/2011GB004224.

Sluijs, A., Brinkhuis, H., Schouten, S., Bohaty, S.M., John, C.M., Zachos, J.C., Reichart, G.-J., Sinninghe Damsté, J.S., Crouch, E.M., and Dickens, G.R., 2007, Environmental precursors to rapid light carbon injection at the Palaeocene/Eocene boundary: Nature, v. 450, p. 1218–1221, https://doi.org/10.1038/nature06400.

Speijer, R.P., Schmitz, B., and van der Zwaan, G.J., 1997, Benthic foraminiferal extinction and repopulation in response to latest Paleocene Tethyan anoxia: Geology, v. 25, p. 683–686, https://doi.org/10.1130/0091-7613(1997)025<0683:BFEARI>2.3.CO;2.

Stassen, P., Dupuis, C., Morsi, A.M., Steurbaut, E., and Speijer, R.P., 2009, Reconstruction of a latest Paleocene shallow-marine eutrophic paleoenvironment at Sidi Nasseur (Central Tunisia) based on foraminifera, ostracoda, calcareous nannofossils and stable isotopes ($\delta^{13}C$, $\delta^{18}O$): Geologica Acta, v. 7, p. 93–112, 10.1344/105.000000273.

Stassen, P., Thomas, E., and Speijer, R.P., 2012, Integrated stratigraphy of the Paleocene-Eocene thermal maximum in the New Jersey Coastal Plain: Toward understanding the effects of global warming in a shelf environment: Paleoceanography, v. 27, p. 1–17, https://doi.org/10.1029/2012PA002323.

Swart, P.K., and Eberli, G., 2005, The nature of the $\delta^{13}C$ of periplatform sediments: Implications for stratigraphy and the global carbon cycle: Sedimentary Geology, v. 175, p. 115–129, https://doi.org/10.1016/j.sedgeo.2004.12.029.

Thomas, E., and Shackleton, N.J., 1996, The Paleocene-Eocene benthic foraminiferal extinction and stable isotope anomalies, *in* Knox, R.W.O'B., Corfield, R.M., and Dunay, R.E., eds., Correlation of the Early Paleogene in Northwest Europe: London, Geological Society London Special Publication 101, p. 401–441, https://doi.org/10.1144/GSL.SP.1996.101.01.20.

Thomas, D.J., Bralower, T.J., and Zachos, J.C., 1999, New evidence for subtropical warming during the Late Paleocene thermal maximum: Stable isotopes from Deep Sea Drilling Project Site 527, Walvis Ridge: Paleoceanography, v. 14, p. 561–570, https://doi.org/10.1029/1999PA900031.

Thomas, D.J., Zachos, J.C., Bralower, T.J., Thomas, E., and Bohaty, S., 2002, Warming the fuel for the fire: Evidence for the thermal dissociation of methane hydrate during the Paleocene-Eocene thermal maximum: Geology, v. 30, p. 1067–1070, https://doi.org/10.1130/0091-7613(2002)030<1067:WTFFTF>2.0.CO;2.

Tripati, A., and Elderfield, H., 2005, Deep-sea temperature and circulation changes at the Paleocene-Eocene thermal maximum: Science, v. 308, p. 1894–1898, https://doi.org/10.1126/science.1109202.

van Hinsbergen, D.J.J., Lippert, P.C., Dupont-Nivet, G., McQuarrie, N., Doubrovine, P.V., Spakman, W., and Torsvik, T.H., 2012, Greater India Basin hypothesis and a two-stage Cenozoic collision between India and Asia: Proceedings of the National Academy of Sciences of the United States of America, v. 109, p. 7659–7664, https://doi.org/10.1073/pnas.1117262109.

Willems, H., Zhou, Z., Zhang, B., and Gräfe, K.-U., 1996, Stratigraphy of the Upper Cretaceous and Lower Tertiary strata in the Tethyan Himalayas of Tibet (Tingri area, China): Geologische Rundschau, v. 85, p. 723–754, https://doi.org/10.1007/BF02440107.

Wing, S.L., Harrington, G.J., Smith, F.A., Bloch, J.I., Boyer, D.M., and Freeman, K.H., 2005, Transient Floral Change and Rapid Global Warming at the Paleocene-Eocene Boundary: Science, v. 310, p. 993–996, https://doi.org/10.1126/science.1116913.

Winguth, A.M.E., Thomas, E., and Winguth, C., 2012, Global decline in ocean ventilation, oxygenation, and productivity during the Paleocene-Eocene Thermal Maximum: Implications for the benthic extinction: Geology, v. 40, p. 263–266, https://doi.org/10.1130/G32529.1.

Zachos, J.C., Wara, M.W., Bohaty, S., Delaney, M.L., Petrizzo, M.R., Brill, A., Bralower, T.J., and Premoli-Silva, I., 2003, A transient rise in tropical sea surface temperature during the Paleocene-Eocene thermal maximum: Science, v. 302, p. 1551–1554, https://doi.org/10.1126/science.1090110.

Zachos, J.C., Röhl, U., Schellenberg, S.A., Sluijs, A., Hodell, D.A., Kelly, D.C., Thomas, E., Nicolo, M., Raffi, I., Lourens, L.J., McCarren, H., and Kroon, D., 2005, Rapid acidification of the ocean during the Paleocene-Eocene thermal maximum: Science, v. 308, p. 1611–1615, 10.1126/science.1109004.

Zachos, J.C., Bohaty, S.M., John, C.M., McCarren, H., Kelly, D.C., and Nielsen, T., 2007, The Palaeocene–Eocene carbon isotope excursion: constraints from individual shell planktonic foraminifer records: Philosophical Transactions of the Royal Society A, Mathematical and Physical Sciences, v. 365, p. 1829–1842, https://doi.org/10.1098/rsta.2007.2045.

Zamagni, J., 2009, Response of a shallow-water ecosystem to the early Paleogene greenhouse environmental conditions [Ph.D. thesis]: Potsdam, University of Potsdam, 120 p.

Zamagni, J., Mutti, M., Ballato, P., and Košir, A., 2012, The Paleocene-Eocene thermal maximum (PETM) in shallow-marine successions of the Adriatic carbonate platform (SW Slovenia): Geological Society of America Bulletin, v. 124, p. 1071–1086, https://doi.org/10.1130/B30553.1.

Zeebe, R.E., Zachos, J.C., and Dickens, G.R., 2009, Carbon dioxide forcing alone insufficient to explain Palaeocene-Eocene Thermal Maximum warming: Nature Geoscience, v. 2, p. 576–580, https://doi.org/10.1038/ngeo578.

Zhang, Q., Willems, H., Ding, L., Gräfe, K.-U., and Appel, E., 2012, Initial India-Asia continental collision and foreland basin evolution in the Tethyan Himalaya of Tibet: Evidence from stratigraphy and paleontology: The Journal of Geology, v. 120, p. 175–189, https://doi.org/10.1086/663876.

Zhang, Q., Willems, H., and Ding, L., 2013, Evolution of the Paleocene–Early Eocene larger benthic foraminifera in the Tethyan Himalaya of Tibet, China: International Journal of Earth Sciences, v. 102, p. 1427–1445, https://doi.org/10.1007/s00531-012-0856-2.

Zhang, Q., Wendler, I., Xu, X., Willems, H., and Ding, L., 2017, Structure and magnitude of the carbon isotope excursion during the Paleocene-Eocene thermal maximum: Gondwana Research, https://doi.org/10.1016/j.gr.2017.02.016.

Science Editor: Bradley S. Singer
Associate Editor: Daniel Clay Kelly

Manuscript Received 24 March 2017
Revised Manuscript Received 21 May 2018
Manuscript Accepted 19 June 2018

Printed in the USA